iScience

CellPress
OPEN ACCESS

Article

Modulation of stress granule dynamics by phosphorylation and ubiquitination in plants

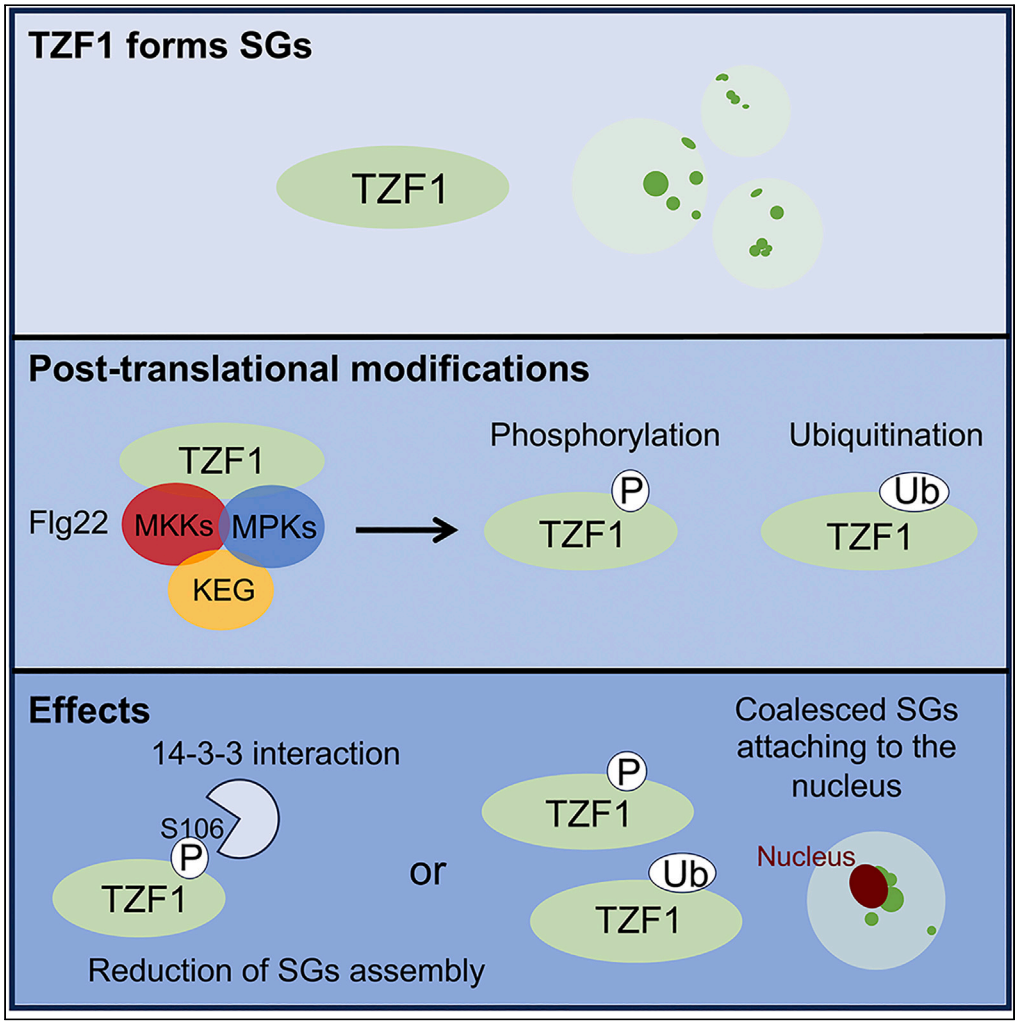

Siou-Luan He, Xiling Wang, Sung-Il Kim, ..., Libo Shan, Ping He, Jyan-Chyun Jang

jang.40@osu.edu

Highlights

TZF1 is a stress granule (SG) protein

TZF1 interacts with MAPK signaling components and E3 ubiquitin ligase KEG in SGs

TZF1 is phosphorylated by MPK3/6 and ubiquitinated by KEG

$TZF1^{P}$ and $TZF1^{Ub}$ differentially modulates SG dynamics in number, size, and location

He et al., iScience 27, 111162
November 15, 2024
https://doi.org/10.1016/j.isci.2024.111162

iScience

CellPress
OPEN ACCESS

Article

Modulation of stress granule dynamics by phosphorylation and ubiquitination in plants

Siou-Luan He,[1] Xiling Wang,[2] Sung-Il Kim,[3] Liang Kong,[3] Ailing Liu,[1,4] Lei Wang,[2] Ying Wang,[5] Libo Shan,[3] Ping He,[3] and Jyan-Chyun Jang[1,6,*]

SUMMARY

The Arabidopsis tandem CCCH zinc finger 1 (TZF1) is an RNA-binding protein that plays a pivotal role in plant growth and stress response. In this report, we show that TZF1 contains two intrinsically disordered regions necessary for its localization to stress granules (SGs). TZF1 recruits mitogen-activated protein kinase (MAPK) signaling components and an E3 ubiquitin ligase KEEP-ON-GOING (KEG) to SGs. TZF1 is phosphorylated by MPKs and ubiquitinated by KEG. Using a high throughput Arabidopsis protoplasts transient expression system, mutant studies reveal that the phosphorylation of specific residues plays differential roles in enhancing or reducing TZF1 SG assembly and protein-protein interaction with mitogen-activated kinase kinase 5 in SGs. Ubiquitination appears to play a positive role in TZF1 SG assembly, because mutations cause a reduction of typical SGs, while enhancing the assembly of large SGs encompassing the nucleus. Together, our results demonstrate that plant SG assembly is distinctively regulated by phosphorylation and ubiquitination.

INTRODUCTION

Ribonucleoprotein (RNP) granules are membrane-less biomolecular condensates normally formed through liquid-liquid phase separation (LLPS) driven by ATP and multivalent protein-protein, protein-RNA, and RNA-RNA interactions. The scaffold proteins in the RNP granules often contain intrinsically disordered domains (IDRs), low-complexity domains (LCDs), or prion-like domains (PrLDs) to facilitate the nucleation and growth of the condensates.[1,2] Processing bodies (P-bodies, PBs) and stress granules (SGs) are two types of RNP granules found in eukaryotic cells. PBs and SGs play crucial roles in physiological and stress responses via the dynamic regulation of signal transduction and mRNA metabolism. PBs and SGs provide a unique spatiotemporal regulatory mechanism that mediates various cellular processes.[1,3–7] Earlier research suggests that PBs and SGs carry out distinct functions, given unique protein and RNA compositions are found in PBs and SGs, respectively. However, the boundaries between PBs and SGs have become blurred with more recent research.[1] Many proteins have been found in both compartments, such as Argonaute 1/2 (Ago1/2), early Initiation Factor 4E (eIF4E), Apolipoprotein B mRNA-editing Enzyme Catalytic polypeptide 1-like 3G (APOBEC3G), and Tristertraprolin (TTP) in non-plant systems,[8,9] and heat shock proteins and RNA helicases in plant system,[2] suggesting overlapping functions and constant dynamic assembly and in some occasions component exchange between PBs and SGs.[1,10]

PBs are constitutive cytoplasmic RNP granules that consist of non-translating mRNAs, mRNA decay factors, translational repressors, and various RNA-binding proteins (RBPs) involved in mRNA storage, degradation, and translational repression.[11] As in mammals, plant PBs contain conserved RNA degradation machinery, such as mRNA decapping factors (DCP1 and DCP2) and 5′-3′ processing exonucleases (XRN4).[9,12] Mutations in genes encoding essential components of PBs in Arabidopsis, such as DCP1 and DCP2, cause growth defects, suggesting an essential role of mRNA decapping in plant development.[12] In addition, PB components are involved in both biotic and abiotic stress responses. For example, microbe-associated molecular patterns (MAMPs) were shown to modulate the dynamic interaction between DCP1, DCP2, and XRN4, assembly of PBs, and selective mRNA decay in plant immunity mediated by mitogen-activated protein kinase (MAPK) signaling cascade.[13] The *Arabidopsis* DCP1 is phosphorylated by mitogen-activated protein kinase 6 (MPK6) and this process is critical for plant dehydration stress tolerance.[14] However, whether MAPK components are recruited to PBs to phosphorylate DCP1 and if PBs are required for dehydration response remain to be addressed.

SGs are another class of cytoplasmic RNP granules that are transiently formed in response to various cellular stressors, such as heat shock, oxidative stress, viral infection, or nutrient deprivation.[1,10,15] When cells encounter stress, translation initiation is often inhibited, leading to the accumulation of untranslated mRNAs. These untranslated mRNAs, along with various RBPs, are the main components for SG assembly. SGs

[1]Department of Horticulture and Crop Science, Center for Applied Plant Sciences, and Center for RNA Biology, The Ohio State University, Columbus, OH 43210, USA
[2]Key Laboratory of Plant Molecular Physiology, Institute of Botany, Chinese Academy of Sciences, and University of Chinese Academy of Sciences, Beijing 10093, China
[3]Department of Molecular, Cellular, and Developmental Biology, University of Michigan, Ann Arbor, MI 48109-1085, USA
[4]College of Bioscience and Biotechnology, Hunan Agricultural University, Changsha 410128, Hunan, China
[5]Plant Pathology Department and Plant Molecular Cellular Biology Program, University of Florida, Gainesville, FL 32611, USA
[6]Lead contact
*Correspondence: jang.40@osu.edu
https://doi.org/10.1016/j.isci.2024.111162

help preserve mRNAs during stress and facilitate their translation after stress relief.[5] In mammals, SGs are typically formed by the aggregation of untranslated mRNAs, stalled translation initiation complexes, small ribosome subunits, and RBPs such as T-cell-restricted intracellular antigen-1 (TIA-1) and Ras-GAP SH3 domain-binding proteins (G3BP1 and G3BP2), as well as many other proteins involved in signal transduction.[16] In plants, the functions of SGs are less well characterized than in mammals, and the dynamics of compositional and functional changes of SGs in response to various cues is also under-investigated. Nevertheless, several plant SG proteins have been identified and characterized based on their homology with animal and yeast proteins or the results of proteomic studies.[2] For instance, Tudor Staphylococcal Nuclease (TSN) proteins have been identified as a core component of plant SGs.[17] The RNA-binding protein 47b (Rbp47b)[18] and oligouridylate binding protein 1B (UBP1B)[19] are the RBPs most closely related to mammalian TIA-1.

Plant tandem CCCH zinc finger proteins (TZFs) have been found in both PBs and SGs.[20] TZFs are evolutionarily conserved in eukaryotes and they are characterized by a TZF motif consisting of two identical CCCH domains (C-X_{7-8}-C-X_5-C-X_3-H) separated by 18 amino acids.[21] However, a unique group of plant TZF proteins contain an arginine-rich (RR) region preceding a variant TZF motif consisting of two distinct CCCH domains (C-X_{7-8}-C-X_5-C-X_3-H-X_{16} and C-X_5-C-X_4-C-X_3-H) called RR-TZF proteins. Genes encoding RR-TZF proteins have been found in numerous higher plants, including *Arabidopsis* (TZF1-11).[22–26] Plant RR-TZF proteins participate in a plethora of biological processes including hormone-mediated growth and stress responses such as leaf senescence (OsTZF1 and OsTZF2),[27,28] ABA/GA-mediated growth and abiotic stress responses (TZF1),[29] seed germination (TZF4/5/6),[30] and flowering time (MsZFN).[31] The mammalian TZF protein TTP is found in PBs and SGs and is participated in the posttranscriptional regulation of gene expression by binding to mRNAs.[32] A classic model of TTP in mRNA regulation has been well established—TTP can trigger the decay of *Tumor Necrosis Factor-α* (*TNF-α*) mRNA by binding to its AU-rich elements (AREs) at 3′-UTR and recruiting deadenylation and decapping complexes to the substrate.[33,34] In plants, TZF1/4/5/6/9,[23] OsTZF1/7,[28,35] and OsC3H10[36] have been reported to colocalize with PBs and SGs markers. TZF1 can directly bind to U rich region of the *Target of Rapamycin* (*TOR*) mRNA at 3′-UTR and trigger *TOR* mRNA degradation.[37] OsTZF1[28] and OsTZF7[35] can bind ARE-like motifs within 3′-UTRs of downregulated target genes and likely induce mRNA turnover.

Although the biophysical mechanisms underpinning the assembly of biomolecular condensates via LLPS have been thoroughly investigated,[1,5] the signal transduction mechanisms that trigger these processes are far from completely understood. Post-translational modifications (PTMs) play a crucial role in the regulation of SG assembly and disassembly. The dynamic nature of SG assembly is closely tied to the PTM status of the scaffold protein components. Alterations in PTMs can impact the formation, stability, and dissolution of SGs in response to cellular stress.[38–40] Phosphorylation is a common PTM that regulates SG dynamics via the impacts on SG protein components. For example, the phosphorylation of TTP by MAPKAP kinase-2 (MK2) promotes its binding to 14-3-3 adaptor proteins, thereby excluding TTP from SGs and stabilizing the ARE-containing target mRNAs.[41] In plants, bacterial flagellin or flg22 peptides induces *Arabidopsis* TZF9 phosphorylation via two MAMP-responsive MPKs, MPK3 and MPK6. Phosphorylation of TZF9 diminishes cytoplasmic granules and RNA-binding properties.[42] In addition, ubiquitination is one of the PTMs that marks proteins for degradation or regulates protein activity. Ubiquitin ligases and deubiquitinating enzymes can influence SG dynamics by modifying the ubiquitination status of key SG proteins.[43,44] The ubiquitination of some SG components may target them for degradation, leading to SG disassembly. For example, G3BP1 undergoes K63-linked ubiquitination in the disassembly of SGs formed under heat stress.[45] Two SG proteins carrying ubiquitin associated (UBA) domains, UBAP2L and UBQLN2, have been found to regulate SG assembly, but their roles are not dependent on the UBA domain.[46,47] These results suggest a role for ubiquitination in regulating SG disassembly, but its impact on SG assembly remains unclear.

In this study, we have demonstrated that Arabidopsis TZF1 is an SG resident protein. Deletion of either or both IDR flanked the RR-TZF motif could almost eliminate the TZF1 SG assembly completely. TZF1 could interact with MAPK signaling cascade components in SGs. TZF1 recruits MPKs to SGs and is phosphorylated by MPK3/6. The potential phosphorylation sites of TZF1 are mapped by mass spectrometry in the absence/presence of a potent MAMP—flg22. Analysis of site-directed single and higher order mutations of potential phosphorylation sites reveal that the phosphorylation of specific residues plays differential roles in enhancing or reducing SG assembly and protein-protein interaction with an MPK3/6 upstream kinase—mitogen-activated kinase kinase 5 (MKK5) in SGs. The mutant analysis also identifies two potential 14-3-3 adaptor protein binding sites to be critical for TZF1 SG assembly and protein-protein interaction with MKK5 in SGs. For the role of ubiquitination, TZF1 protein accumulates at a lower level in a gain-of-function *keg-4*[48,49] mutant plant and TZF1 is ubiquitinated by KEEP-ON-GOING (KEG). Remarkably, ubiquitination played a positive role in SG assembly, because single or higher order mutations on predicted ubiquitination sites of TZF1 reduced the number of SGs per cell, while enhancing the coalescence of small SGs into a large single SG attaching to the nucleus. Together, our results demonstrate that the assembly of TZF1 into SGs is mediated by a wide array of PTM mechanisms, in which ubiquitination and phosphorylation play a distinct role.

RESULTS

Arabidopsis protoplast transient expression as a high throughput tool to study ribonucleoprotein granule dynamics

We have shown previously that TZF1 is mainly localized in the cytoplasmic condensates, and it can co-localize with both PB (DCP2) and SG (PABP8) markers. TZF1 condensates display a characteristic property of RNP granules that can be disassembled by cycloheximide (CHX) treatment within 15 min.[50] In intact transgenic plants, TZF1 condensates are found only in specific tissues/cells and often require the induction by stress cues such as methyl jasmonate (MeJA)[50] and salt.[51] TZF condensates induced by MeJA are consistent in both intact plants and isolated mesophyll protoplasts and this could also be seen in intact plants expressing a construct driven by the native *TZF6* promotor.[30] Nevertheless, the rarity, tissue heterogeneity, and induction requirement present a challenge for a large-scale investigation of the effects of the PTM of TZF1 in the dynamics of SG assembly/disassembly in the current study. Using a meticulous Arabidopsis transient expression system[52,53] in which

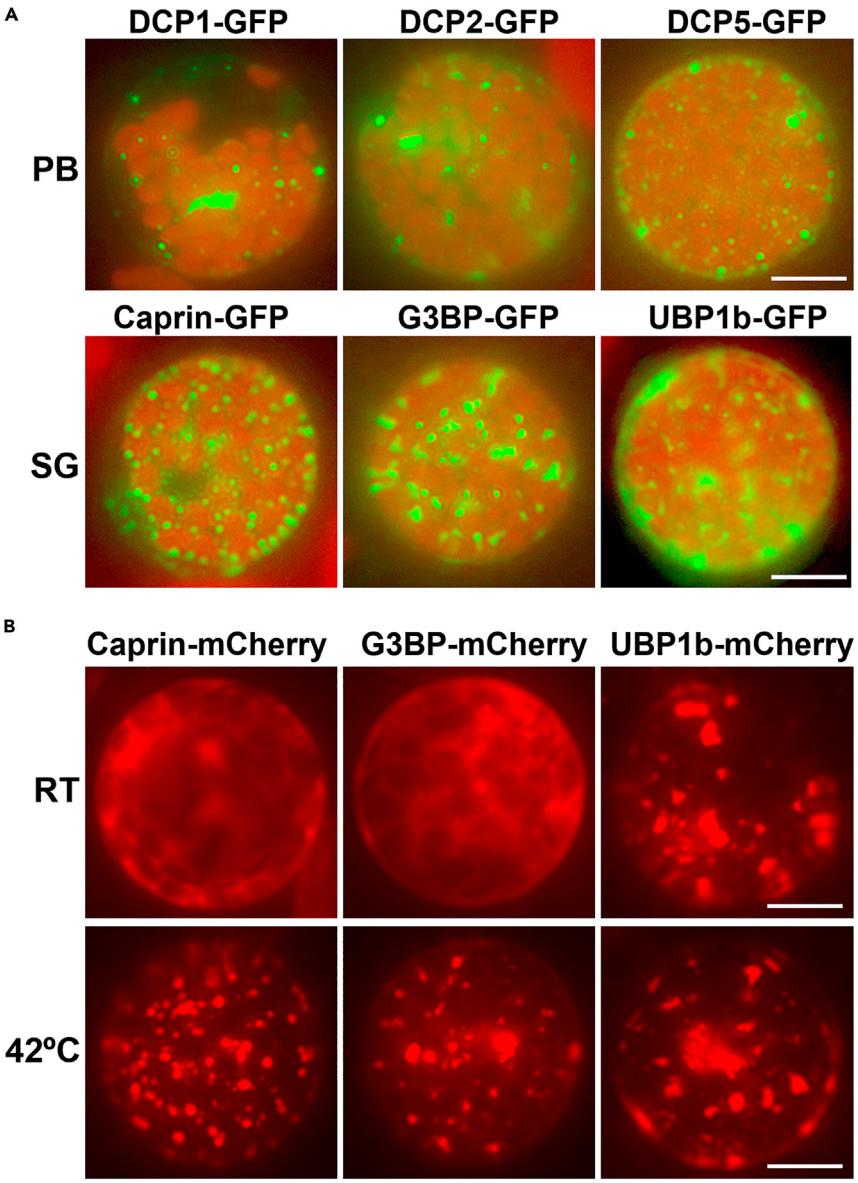

Figure 1. RNP granule dynamics in Arabidopsis protoplasts transient expression system

(A) Fluorescent microscopy images showing the droplet morphology of PB markers DCP1, DCP2, and DCP5, and SG markers Caprin, G3BP, and UBP1b. Protoplasts expressing SG markers were heat shock at 42°C for 5 min before imaging. The green fluorescence was viewed under a B-2A blue excitation filter. Background red color was emitted from chloroplast auto-fluorescence. Scale bar = 10 μm.

(B) Except for UBP1b, most SG markers, such as Caprin and G3BP, are stress-inducible (e.g., by heat shock at 42°C for 5 min) in Arabidopsis protoplasts. The mCherry red fluorescence was viewed under the Y-2E/C yellow excitation filter. Scale bar = 10 μm.

mesophyll protoplasts were isolated consistently from the 8th leaf (0.8–1.2 × 1.0–1.5 cm, highlighted in red rectangle) of 3-week-old plants (Figure S1A), protein expression results could be achieved with high efficiency and reproducibility. For example, transformation efficiency for different fusion protein genes such as *CaMV35S:GFP* (Figure S1B) and *CaMV35S:NLS-RFP* (Figure S1C) could reach as high as 90%. Such a system allowed the observation of hundreds of cells in a single experiment. Remarkably, TZF1-GFP fusion protein could be localized consistently to cytoplasmic granules without additional drug or stress treatments (Figure S1D).

In addition to TZF1, several PB and SG markers were also tested in the protoplast system. The three PB (DCP1, DCP2, and DCP5) and SG (Caprin, G3BP, and UBP1b) components displayed typical droplet-like morphology of RNP granules in transiently expressed Arabidopsis protoplasts (Figure 1A). In contrast to PB markers, heat shock treatment at 42°C for 5 min was required for SG assembly. The three SG markers fused with a different fluorescence tag (mCherry) were also tested. Consistent with GFP fusion SG markers, both Caprin-mCherry and G3BP-mCherry required heat shock for SG assembly, whereas UBP1b-mCherry could be spontaneously assembled into SGs in the protoplasts

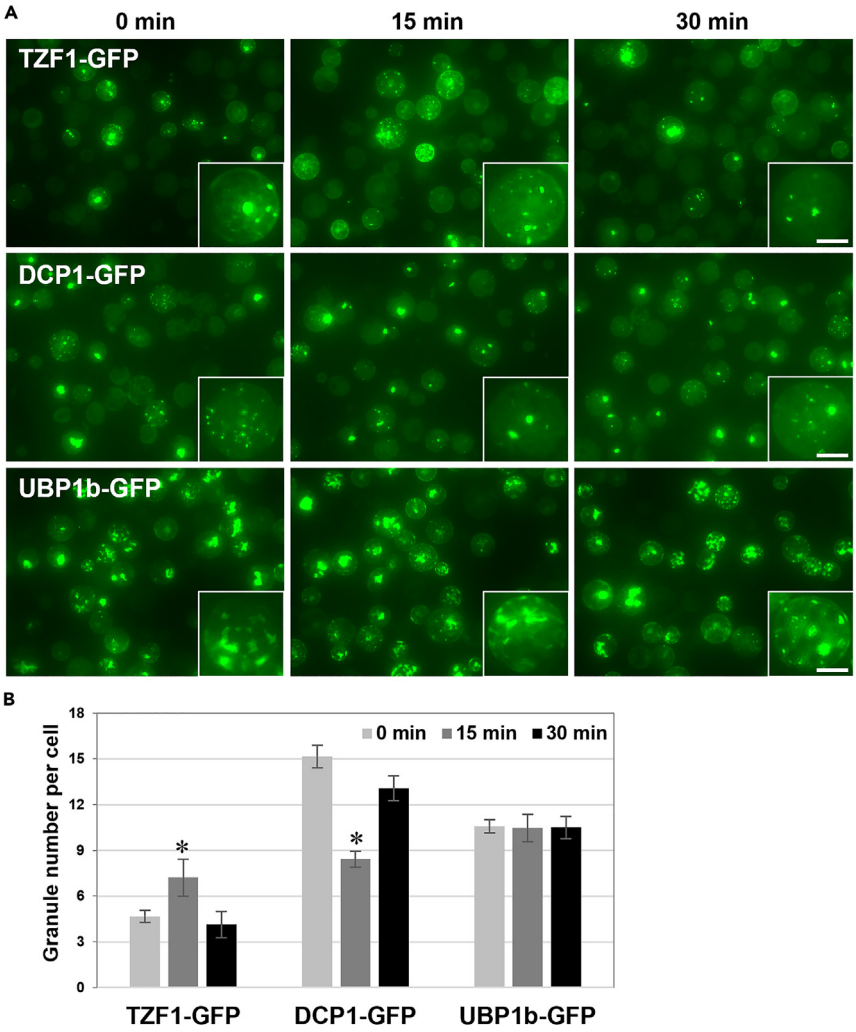

Figure 2. Cytoplasmic granule dynamics in response to flg22

(A) Arabidopsis protoplasts were transiently expressed with indicated DNA constructs, incubated overnight, and treated with synthetic bacterial flagellin flg22 (0.1 μM) for 15 and 30 min, respectively, before fluorescence microscopy analysis. Typical single cell of each sample population is shown in the insert. Scale bar = 10 μm.

(B) Quantitative analysis of granule number per cell as shown in (A). Columns represent means ± *SE* (*n* = 100). Asterisks indicate significant differences from 0 min (*, $p < 0.05$) by Student's t test.

(Figure 1B). Given both Caprin and G3BP could also interact directly with MKK4 and MKK5 (results not shown), UBP1b was used as an SG marker for the rest of the study.

In a previous report, we showed that the assembly of DCP1-associated PBs was dynamically regulated by flg22 in Arabidopsis protoplasts.[13] Upon flg22 treatment, DCP1-GFP granules started to disappear in 15 min and were dropped to the lowest level in 30 min before reappearing in 60 min and restoring to the full level as untreated in 120 min. In contrast to DCP1 granules, the number of TZF1 granules appeared to increase within the first 15 min of flg22 treatment and resume to a normal number at 30 min in the protoplasts (Figure 2). The number of granules associated with SG marker UBP1b remained nearly constant during the time course experiment. These results suggest that the assembly/disassembly of PBs or SGs associated with a specific protein could be post-translationally and differentially regulated by flg22. Given that TZF1 SGs could still be disassembled by CHX[50] or flg22 (Figure 2)[13] treatment and further induced by MeJA and heat (results not shown), the Arabidopsis protoplast transient expression system appeared to be an ideal tool to complement the intact plant system in the current study.

Tandem CCCH zinc finger 1 is a stress granule component

Although TZF proteins were shown to co-localize with PB marker DCP2,[30] a later report indicated that DCP2 was not a PB-specific marker.[51] We therefore re-examined the sub-cellular localization of TZF1 using a set of different markers. The TZF1-GFP fusion protein is functional as reported recently.[51] Results showed that TZF1 could only partially co-localize with a major PB component DCP1, but completely co-localize

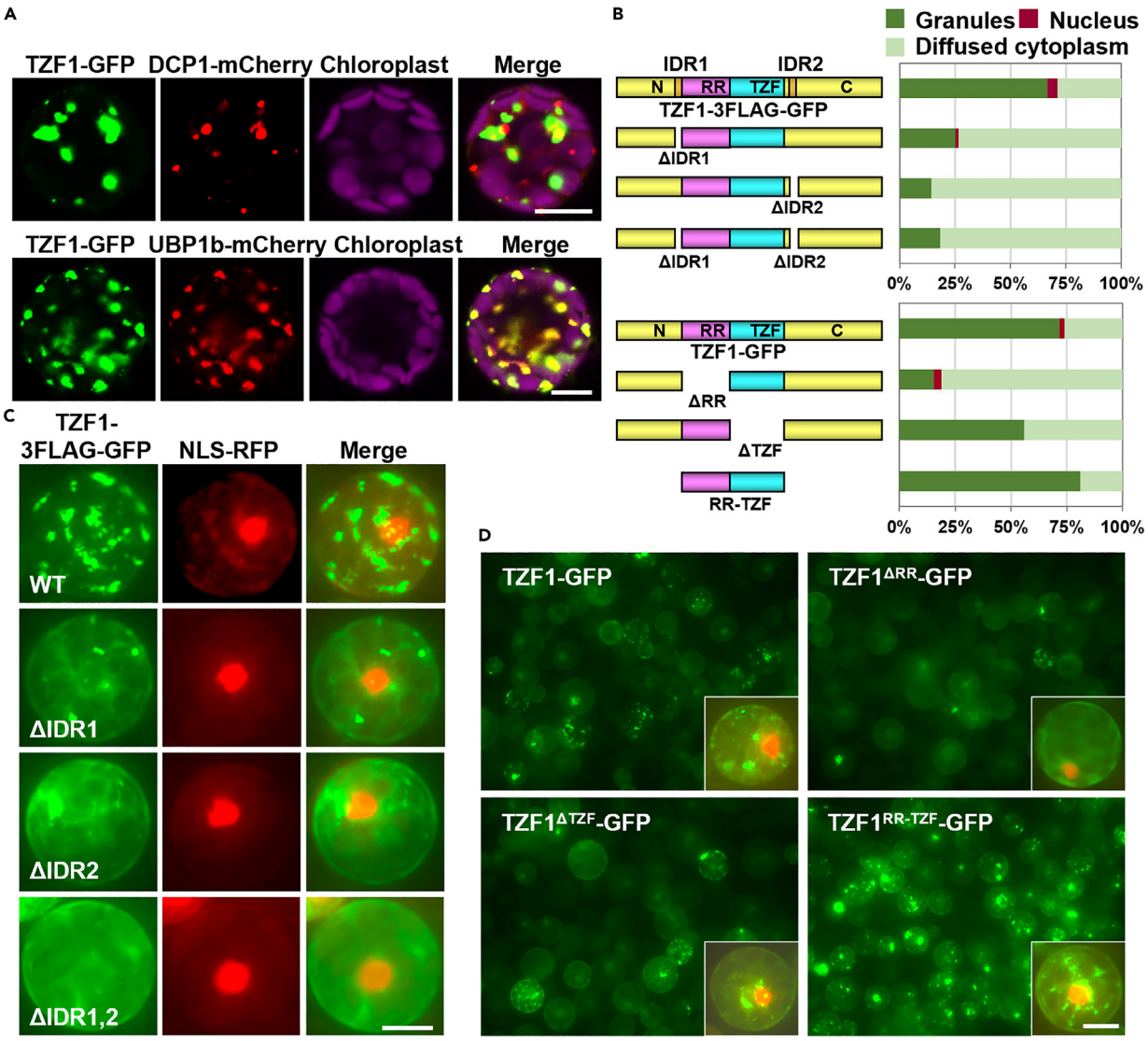

Figure 3. TZF1 is a stress granule component

(A) Confocal imaging showing that TZF1 is localized in cytoplasmic condensates and partially co-localized with PB marker DCP1, whereas completely co-localized with SG marker UBP1b. Scale bar = 10 μm.

(B) The intrinsically disordered regions (IDR1 and IDR2) and RR-TZF motif are required for TZF1 cytoplasmic granule localization. Schematic representation of DNA constructs with the deletion of predicted IDR (ΔIDR) and RR-TZF motif (ΔRR or ΔTZF) and corresponding statistical analysis of TZF1 subcellular localization patterns. Total number of cells counted $n > 250$ for each construct.

(C) TZF1 cytoplasmic granules were significantly reduced with IDR deletions. Scale bar = 10 μm.

(D) TZF1 cytoplasmic granules were reduced by the deletion of RR or TZF but increased when only RR-TZF was present. Image in the insert is a single cell co-expressed with TZF1-GFP and NLS-RFP. Scale bar = 10 μm.

with SG marker UBP1b (Figure 3A). Although DCP1 has also been found as a non-specific PB marker in plants recently,[54] it is minimal co-localization with TZF1 suggesting that TZF1 is more likely or more often an SG component, as it completely co-localizes with various SG markers.[51] IDRs are the key drives to trigger the assembly of biomolecular condensates within cells.[1,2] These condensates play critical roles in cellular organization, signaling, and gene regulation and abnormal condensate assemblies have been implicated in various diseases.[5] The mammalian TZF1 homolog TTP is both an RBP and an IDR scaffold protein for SG assembly.[41] Using SMART (http://smart.embl-heidelberg.de/) and Iupred2A (https://iupred2a.elte.hu/) algorithms, two IDRs were identified in TZF1 protein. Deletion constructs of $TZF1^{\Delta IDR1}$ (aa 70–85, upstream of RR), $TZF1^{\Delta IDR2}$ (aa 218–233, downstream of TZF), and $TZF1^{\Delta IDR1,2}$ were then made accordingly (Figure 3B). Remarkably, the deletion of either or both IDR strongly reduced TZF1 SG assembly (Figures 3B and 3C), despite the truncated proteins being accumulated at the similar levels to that of the WT (Figure S2A).

As it was shown that RR-TZF domain of TZF1 protein is required for high-affinity RNA binding,[55] the effects of TZF1$^{\Delta RR}$, TZF1$^{\Delta TZF}$, and TZF1^{RR-TZF} (Figure 3B) on TZF1 SG assembly were examined. Deletion of either RR or TZF caused a severe reduction of TZF1 SG assembly. The RR-TZF fragment alone conferred strong SG assembly (Figures 3B and 3D), suggesting that both either N- or C-terminus contains negative elements for SG assembly. Results of immunoblot analysis indicated that reduced TZF1 SG granule assembly caused by ΔRR and ΔTZF was not due to reduced protein accumulation (Figure S2B), indicating that TZF1 SG assembly is mediated through post-translational regulatory mechanisms.

Tandem CCCH zinc finger 1 interacts with mitogen-activated protein kinase signaling components

To further explore the interacting proteins in the TZF1 protein complex, immunoprecipitation coupled with mass spectrometry (IP-MS) was performed using transgenic plants ectopically expressing *CaMV35S:TZF1-GFP*.[29] Notably, two upstream kinases of MAPK, MKK4, and MKK5, two 14-3-3 adaptor proteins, an E3 ubiquitin ligase KEG, and a conserved SG marker DEAD-box containing RNA helicase (RH6/8/12) were among the candidates identified by IP-MS (Figure 4A). Coincidentally, KEG was found to ubiquitinate MKK4 and MKK5 in modulating plant immunity.[48] As we demonstrated previously that MAPK cascades (e.g., MPK3/6 and MKK4/5) are involved in MAMPs orchestrated PB dynamics,[13] additional analyses were conducted to validate TZF1 protein-protein interaction with MAPK signaling components. Results showed that TZF1 could interact with MPK3, MPK6, MKK4, and MKK5 in both yeast-two-hybrid (Y-2-H) (Figure 4B) and co-immunoprecipitation (Co-IP) (Figure 4C) analyses. Consistent with TZF1's sub-cellular localization, protein-protein interaction of TZF1-MPK3, TZF1-MPK6, and TZF1-MKK5 occurred in droplet-like cytoplasmic condensates in bi-molecular fluorescence complementation (BiFC) analyses (Figure 4D). These protein complexes were only partially co-localized with PB marker DCP1 but completely co-localized with SG marker UBP1b in BiFC analyses (Figure S3). Neither TZF1-nYFP nor TZF1-cYFP could interact with its corresponding BiFC empty vector construct. However, the MPK3-cYFP, MPK6-cYFP, and MKK4-cYFP did produce very weak nuclear signals with the nYFP empty vector. The MKK5-cYFP and nYFP empty vector generated slightly more visible YFP signals in the nuclei but never occurred in the cytoplasmic granules (Figure S4A), indicating that the nuclear signals were likely artifacts in the BiFC system. To further confirm the specificity of the BiFC results, additional negative controls were included. Results showed that while MKK5-cYFP interacted with TZF1-nYFP in the cytoplasmic granules, it could not interact with five other nYFP fusion proteins (Figure S4B), indicating the specificity of TZF1 interaction with MAPK signaling components.

The BiFC results prompted us to examine the sub-cellular localization of MAPK signaling components. Using various fluorescence protein markers, we found that MKK4 and MKK5 were mainly localized in the cytoplasmic condensates, whereas MPK3 and MPK6 were mainly localized in the nucleus and cytoplasm (Figure 5A). Consistently, the MKK4-GFP and MKK5-GFP were localized in the cytoplasmic condensates in transgenic plants, albeit the nuclear signals were also visible (Figure 5B). Interestingly, individual MPK3, MPK6, MKK4, and MKK5 were not co-localized with PB marker DCP1, but completely co-localized with SG marker UBP1b (Figure S5). Given TZF1-MPK3, TZF1-MPK6, TZF1-MKK4, and TZF1-MKK5 were not colocalized well with PB marker but completely co-localized with SG marker (Figure S3), these results raise a possibility that MAPK cascade components are normally localized in nucleus, cytoplasm, or SGs to a lesser extent. MPK3/6 and MKK4/5 are recruited mainly to SGs when interacting with TZF1 (Figure 5C).

Tandem CCCH zinc finger 1 is phosphorylated by mitogen-activated protein kinase 3/6

The interaction between TZF1 and MAPK signaling components prompted us to determine if TZF1 could be phosphorylated by MPKs. Results of Phos-tag SDS-PAGE analysis indicated that TZF1 could be phosphorylated by MPK3, MPK4, and MPK6 upon flg22 treatment (Figure 6A). The human TZF TTP is known to be heavily phosphorylated in numerous sites[56] and the phosphorylation status affects its subcellular localization, stability, and function.[57] We then performed phosphosite mapping by liquid chromatography coupled with tandem mass spectrometry (LC-MS/MS) to identify potential phosphorylation sites in TZF1. The eight identified phosphopeptides corresponded to ten residues S71, S73, S74, S80, S106, T110, S254, S266, T276, and S296 in TZF1 (Figures 6B, 6C and 7). Among which, four sites (S71, S73, S80, and S254) were phosphorylated in the presence of flg22, with S80 showing the highest probability score and it was also predicted as a conserved MPK phosphosite with a signature SP motif. Three sites (S74, T110, and S296) appeared to be de-phosphorylated in the presence of flg22, with S74 showing the highest probability score. This might be of interesting because S74 clustered with three other flg22-induced phosphorylation sites S71, S73, and S80. The phosphorylation status of three additional sites (S106, S266, and T276) did not seem to be affected by the flg22 treatment. Notably, S106 and T276 were within a predicted 14-3-3 adaptor protein interacting site, respectively (Figure 6C).

It has long been documented that the phosphorylation of TTP by the P38^{MAPK}-MK2 signaling cascade prevents TTP localization to SGs and triggers protein-protein interaction between TTP and 14-3-3 protein.[57,58] We therefore mutated S and T residues to A (phosphor-dead) or D (phosphor-mimetic) on the putative phosphorylation sites by site-directed mutagenesis to generate TZF1-3FLAG-GFP and TZF1-nYFP (BiFC) construct for sub-cellular localization and protein-protein interaction analysis, respectively. For the TZF1 (WT)-3FLAG-GFP, the majority (~70%) of the cells showed a typical SG pattern (Figures S1D and 8A #1). A small percentage of the cells displayed diffused cytoplasmic (Figure 8A #2), nuclear (Figure 8A #3), or nucleus-like (Figure 8A #4) pattern, consistent with our previous report that TZF1 can traffic between nucleus and cytoplasm/cytoplasmic foci in Arabidopsis leaf mesophyll protoplasts.[50] It was intriguing that cells with a reduced number of SGs appeared to be correlated with the formation of a large, aggregate-like, coalesced SG not co-localized but often overlapped with the nucleus (Figure 8A #4). Confocal microscopy rotating view of the large SG-nucleus complex revealed that the two organelles were in close proximity (Videos S1 and S2). It was unclear from the image whether they were physically attached. Noticeably, the large coalesced TZF1 granules were completely co-localized with the SG marker UBP1b (Figure 8B), illustrating the dynamic assembly of TZF1 SGs in various cells. Although mesophyll protoplasts isolated from a specific leaf appeared to be quite uniform in morphology (Figure S1), cellular heterogeneity

A

AGI code	Accession	Description	Mascot score #1	Mascot score #2	Mascot score #3
At2g25900	O82307	TZF1	1384	686	395
At5g13530	Q9FY48	E3 ubiquitin-protein ligase KEG	70	44	39
At1g51660/At3g21220	O80397/Q8RXG3	Mitogen-activated protein kinase kinase 4/5 MKK4/5	56	ND	64
At2g45810/At3g61240/At4g00660	Q94BV4/Q9M2E0/Q8RXK6	DEAD-box ATP-dependent RNA helicase family protein RH6/8/12	33	ND	56
At1g78300	Q01525	14-3-3-like protein GF14 omega	79	ND	ND
At5g38480	P42644	14-3-3-like protein GF14 psi	64	ND	ND

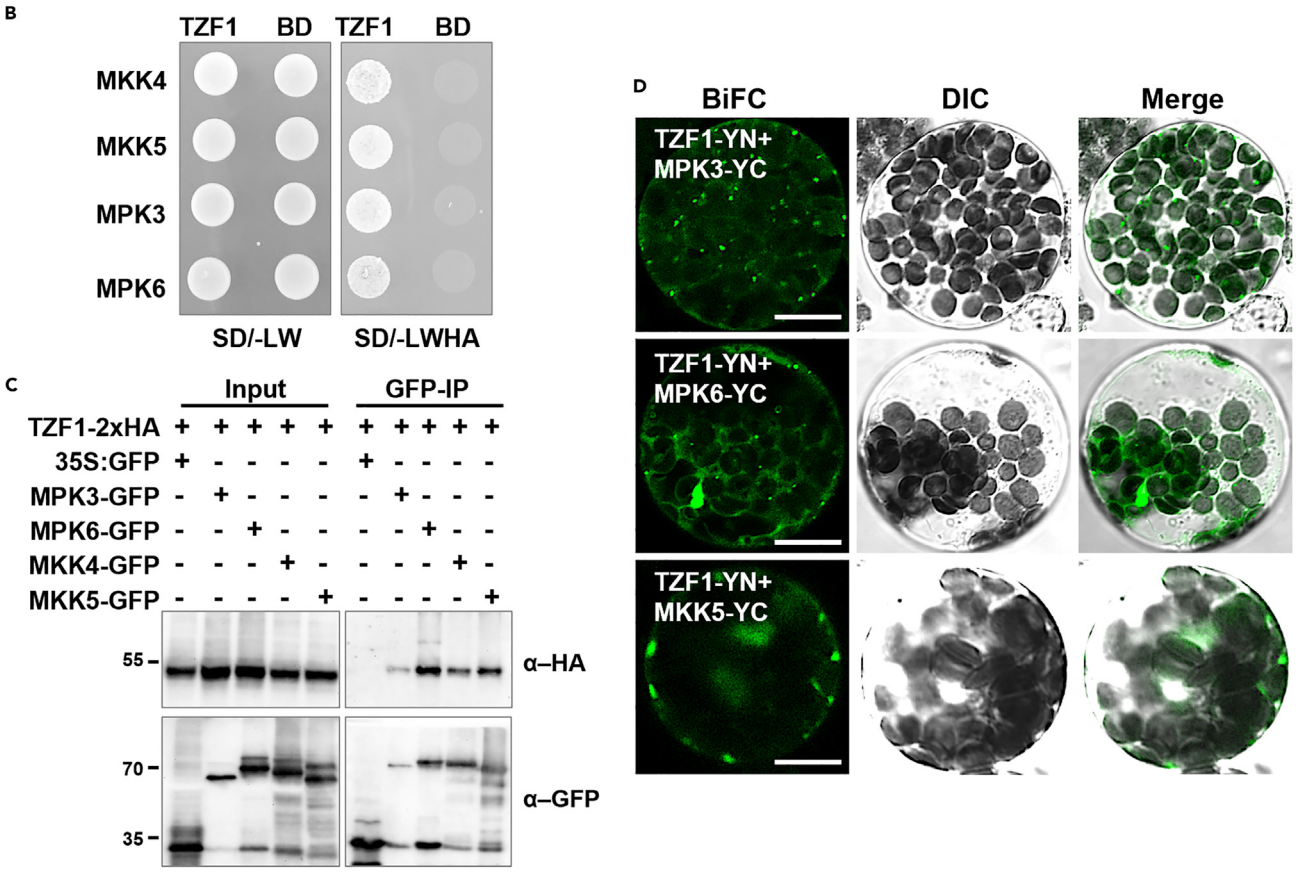

Figure 4. TZF1 interacts with MAPK signaling components

(A) Selected TZF1 protein complex components identified by immunoprecipitation coupled mass spectrometry (IP-MS).

(B) TZF1 interacts with MAPK signaling components MKK4, MKK5, MPK3, and MPK6 in a Y-2-H assay, as indicated by the yeast growth on the quadruple amino acids dropout (-LWHA) selection plate. BD: empty vector with a GAL4 binding domain was used as a negative control.

(C) Co-IP analysis results indicate that TZF1 interacts with MPK3, MPK6, MKK4, and MKK5. Arabidopsis protoplasts were co-expressed with indicated constructs and IP was performed using anti-GFP antibody and immunoblot was carried out using anti-HA and anti-GFP antibody, respectively.

(D) Confocal microscopy images showing that TZF1 interacts with MPK3/6 and MKK5 in cytoplasmic granules in BiFC analysis. Scale bar = 10 μm.

existed due to developmental and physiological gradients in the whole leaf. This was fully supported by recent findings in which auxin response factor (ARF) cytoplasmic condensates regulate auxin responsiveness in a developmental gradient in the root system.[59] Furthermore, DCP1 protein condensates are differentially accumulated at the edges and vertices of root cells in different regions to cooperate with the actin nucleating complex to regulate actin remodeling.[60] Therefore, a certain level of variation in the TZF1 granule pattern could be due to developmental cues rather than the mutation alone (see later in discussion mutant analyses). Nevertheless, such variation is also expected to occur in the intact plants. On the basis of the results so far, we hypothesized that TZF1 granule patterns could be modulated by both external and internal cues, including the PTM of TZF1 protein itself.

For flg22-induced phosphorylation sites (S71, S73, S80, and S254), most mutations caused the reduction of TZF1 SGs, particularly S80, a conserved MPK phosphorylation site. Both S80A and S80D significantly reduced TZF1 SG assembly, in contrast to S254A with reduction and S254D with little change. The higher-order mutations (71/73/80 and 71/73/80/254) did not reduce the ratio of cells with SGs, while causing the coalescence of SGs to form larger condensates (Figures 8C and 8G). For flg22-induced de-phosphorylation sites (S74, T110, and

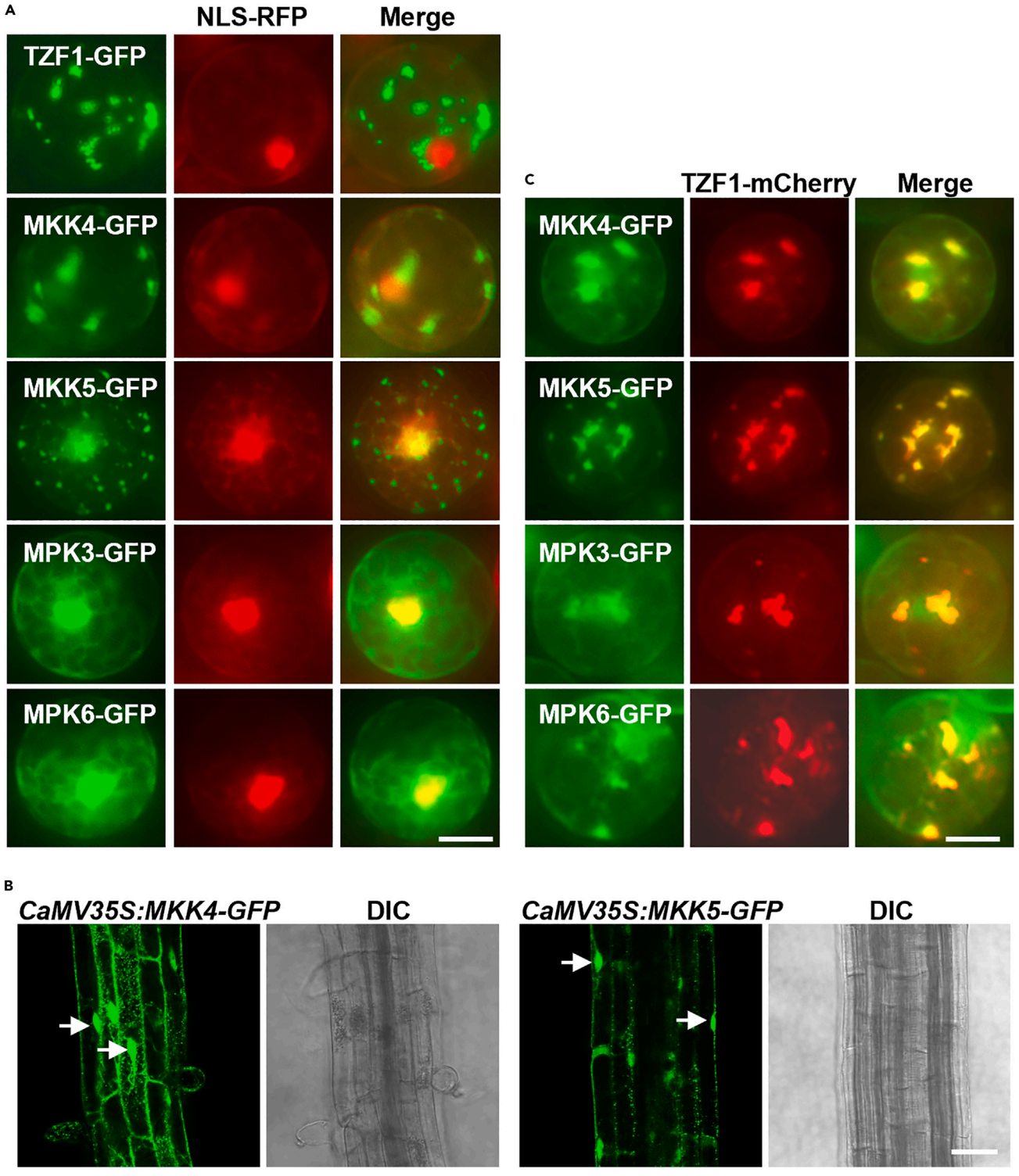

Figure 5. Subcellular localization of TZF1 and MAPK signaling components

(A) TZF1, MKK4, and MKK5 are localized in cytoplasmic condensates, whereas MPK3 and MPK6 are mainly localized in the nucleus in Arabidopsis protoplasts. NLS-RFP, a marker for nuclear proteins. Scale bar = 10 μm.

(B) MKK4 and MKK5 are localized in cytoplasmic condensates in stable transgenic Arabidopsis plants. Shown are root tissues with GFP signals in cytoplasmic condensates throughout the cells and in the nuclei (arrows). Scale bar = 10 μm.

(C) MPK3, MPK6, MKK4, and MKK5 co-localize with TZF1 in Arabidopsis protoplasts. Scale bar = 10 μm.

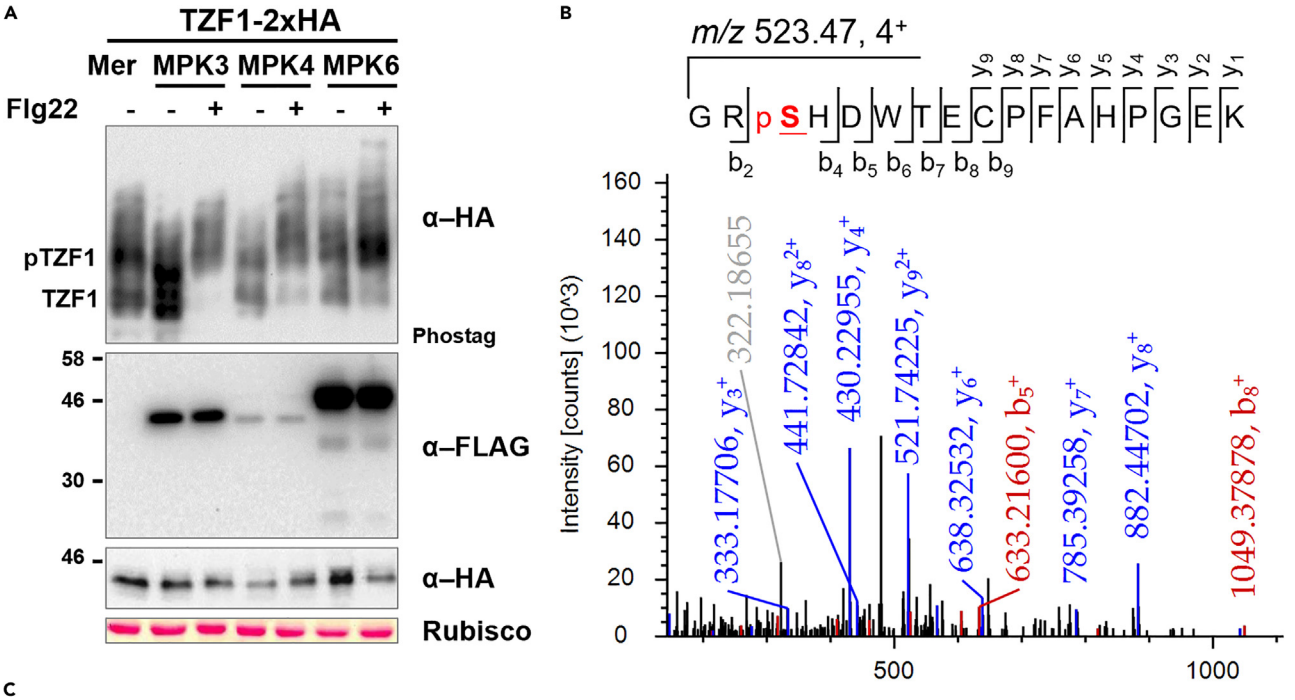

C

Peptide	PSM TZF1_H2O	PSM TZF1_flg22	Peptide position	Phos-site position
[R].GRpSHDWTECPFAHPGEK.[A]	2	3	104-120	S106
[R].LPFpSSLRPIQAApTWPR.[I]	5	6	263-279	S266 T276
[R].YLPSNELTNDSDSpSSGDESSPLTDSFSSDEFR.[I]	10	0	61-92	S74
[R].SHDWpTECPFAHPGEK.[A]	2	0	106-120	T110
[R].IREFEIEEAPAMEFVEpSGKELR.[A]	2	0	280-301	S296
[R].YLPSNELTNDpSDpSSSGDESSPLTDSFSSDEFR.[I]	0	2	61-92	S71 S73
[R].YLPSNELTNDSDSSSGDESpSPLTDSFSSDEFR.[I]	0	7	61-92	S80
[K].MQLNGGGCSWpSSPMR.[S]	0	2	244-258	S254

Figure 6. Flg22 induces the phosphorylation of TZF1 on multiple serine and threonine residues

(A) Flg22-activated MPK3, MPK4, and MPK6 phosphorylate TZF1 in Arabidopsis protoplasts. Protoplasts co-expressing TZF1-HA with MPK3-FLAG, MPK4-FLAG, or MPK6-FLAG were treated with or without 0.1 μM flg22 for 15 min. Total proteins were separated with Mn^{2+}-Phos-tag and regular SDS-PAGE gels, followed by immunoblot analysis with α-HA or α-FLAG antibodies. Protein loading is shown by Ponceau S staining for rubisco.

(B) LC-MS/MS spectrum of a phosphorylated peptide containing Ser-106 in TZF1 ($TZF1^{S106}$). Protoplasts expressing TZF1-HA were treated without (H_2O) or with 0.1 μM flg22 for 10 min. TZF1-HA was immunoprecipitated with α-HA magnetic beads and separated by SDS-PAGE gel, followed by digestion with trypsin and LC-MS/MS analysis to identify TZF1 phosphorylation sites.

(C) List of TZF1 phosphorylation peptides identified by LC-MS/MS analysis. The peptide-spectrum match (PSM) indicates the number of identified phosphorylated peptides. $TZF1^{S74}$, $TZF1^{T110}$, and $TZF1^{S296}$ were only identified in the H_2O sample (pink boxes). $TZF1^{S71}$, $TZF1^{S73}$, $TZF1^{S80}$, and $TZF1^{S254}$ were only identified in the flg22-treated sample (green boxes). $TZF1^{S106}$, $TZF1^{S266}$, and $TZF1^{T276}$ were identified in both H_2O and flg22-treated samples (gray boxes).

S296), except for S74A showing a slight decrease of SG assembly, none of the other mutants showed any significant change in the percentage of cells showing SG pattern (Figures 8D and 8G). Notably, the quadruple mutant of S71/73/74/80A caused an increase, whereas S71/73/74/80D caused a decrease in SG assembly (Figures 8E and 8G). Finally, the predicted MPK phosphorylation site mutation of either S255A or S255D along with the double mutants of S254/255A or S254/255D caused a significant reduction of SG assembly, although TZF1 granules in the double mutants appeared to be larger in size (Figures 8F and 8G). Given that the large aggregates-like TZF1 granules only presented in a small percentage of the cells expressing *$TZF1^{WT}$-GFP*, but accounted for much higher ratios in various mutants such as *$TZF1^{S254/255D}$-GFP* and *$TZF1^{S71/73/80/254D}$-GFP* (Figures 8C and 8F), the phosphorylation status of TZF1 appeared to be able to modulate TZF1 SG morphology.

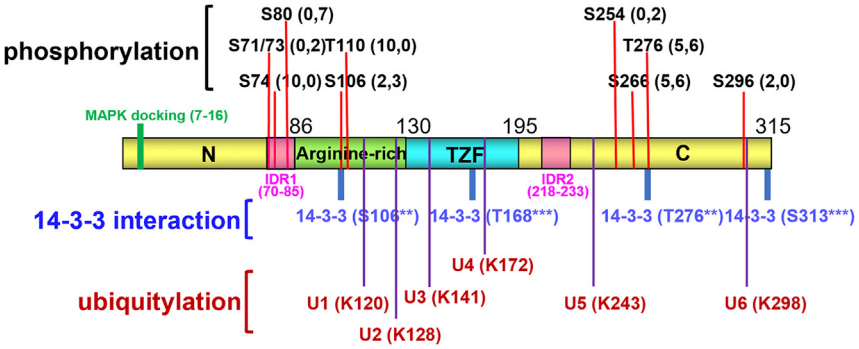

Figure 7. Schematic representation of domain structures and predicted post-translational modifications of TZF1

TZF1 is roughly divided into the N-terminus (N), arginine-rich motif (RR), tandem CCCH zinc finger motif (TZF), and C-terminus (C). The predicted MAPK docking site (aa 7 to 16) and two intrinsically disordered domains (IDR1 and IDR2) are also shown. Residues in black are predicted phosphorylation sites revealed by LC/MS-MS analysis. The two numbers in the parentheses next to the indicated residue are the peptide spectrum match (PSM) scores for samples treated without and with flg22, respectively. Residues in blue are potential 14-3-3 protein-protein interaction sites predicted by 14-3-3-Pred algorithm (https://www.compbio.dundee.ac.uk/1433pred). Residues in red are potential ubiquitination sites predicted by BDM-PUB (Computational Prediction of Protein Ubiquitination Sites with a Bayesian Discriminant Method).

As TZF1 SG patterns in the higher-order mutants were not necessarily an additive outcome of the single mutants, these results also indicated that protein phosphorylation plays a differential role in TZF1 SG assembly and there appears to be close interactions between phosphorylation events at different sites. For TZF1 protein accumulation, flg22-induced phosphorylation site phosphor-dead mutations (S80A, S254A, S71/73/80A, S71/73/80/254A) caused an increase (Figure S6A), whereas the corresponding phosphor-mimetic mutations (S to D change) caused a slight decrease of TZF1 protein accumulation (Figure S6B). For flg22-induced de-phosphorylation sites, the phosphor-dead mutations (S74A, T110A, S74/T110A, S296A) did not appear to affect, while the corresponding phosphor-mimetic mutations caused a significant reduction of TZF1 protein accumulation (Figure S6). Finally, S255D and S254/255D mutants also caused a drastic reduction of TZF1 protein accumulation. Together, these results suggest that de-phosphorylation causes an increase, whereas phosphorylation causes a decrease in TZF1 protein accumulation. For protein-protein interaction, neither flg22-induced phosphorylation nor de-phosphorylation mutations affect TZF1 interaction with MKK5 in SGs (Figure S7), albeit variations were observed in the number and size of SGs (where TZF1 and MKK5 interacted) per cell.

The effects of 14-3-3 adaptor protein interaction sites

The IP-MS results indicated that TZF1 could potentially interact with two 14-3-3 adaptor proteins (Figure 4A). Using a 14-3-3-Pred algorithm, 29 potential 14-3-3 protein interacting sites were predicted in TZF1. Among them S106, T168, T276, and S313 had the highest scores (Figure 9A). Because S106 fell within the RR domain and T168 fell within the TZF domain, site-specific mutations were made to test if these sites were important for TZF1 subcellular localization and protein-protein interaction. The S to A change (phosphor-dead to block 14-3-3 adaptor protein interaction) appeared to enhance the intensity of TZF1 SG signals (Figure 9B), although the percentage of cells with SGs remained largely unchanged (Figure 9C). Because S106 was identified as a phosphorylation site, the phosphor-mimetic mutant S106D was also examined. Interestingly, S106D significantly reduced the TZF1 SG assembly (Figures 9B and 9C), implicating that the interaction with 14-3-3 adaptor protein via S106 could potentially cause TZF1 SG disassembly via an as-yet-unknown mechanism. By contrast, T168A and S106T168A appeared to enhance TZF1 SG assembly (Figures 9B and 9C), suggesting that 14-3-3 interaction with TZF1 via T168 might play a negative role in TZF1 SG assembly. Immunoblot analysis revealed that the mutant proteins, including S106D, appeared to accumulate at higher levels than the WT TZF1 protein (Figure 9D). For protein-protein interaction, S106A appeared to reduce, whereas T168A and S106/T168A mutations appeared to enhance the interaction between TZF1 and MKK5 in larger coalesced SGs (Figure S8). Therefore, it is likely that TZF1's S106 plays a positive and T168 plays a negative role for 14-3-3 mediated TZF1-MKK5 interaction in SGs. The mechanism by which S106 and T168 affect TZF1-MKK5 interaction is currently unknown and will be determined in future studies.

Tandem CCCH zinc finger 1 protein accumulation is affected by KEEP-ON-GOING

Given KEG is associated with MKK4 and MKK5[48] and all three components were also identified in our IP-MS analysis (Figure 4A), the functional relationship between TZF1 and KEG was investigated. Although KEG was reported to be localized in the trans-Golgi network and early endosomes,[61] it could partially co-localize with TZF1 in cytoplasmic condensates (Figure 10A). TZF1 protein stability was then examined. In 7-day-old *CaMV35S:TZF1-GFP* (*TZF1-OX*) transgenic plants, TZF1 protein was very unstable—it almost completely disappeared after being treated by protein synthesis inhibitor CHX for just 1 h. By contrast, its accumulation was restored by the treatment of proteosome inhibitor MG115/132 cocktail. TZF1 accumulation could also be stabilized by PYR41, a ubiquitin-activating enzyme E1 inhibitor, or the combination of MG115/132 and PYR41 (Figure 10B). Consistently, TZF1 cytoplasmic granules were enhanced by MG132 in the root cells of

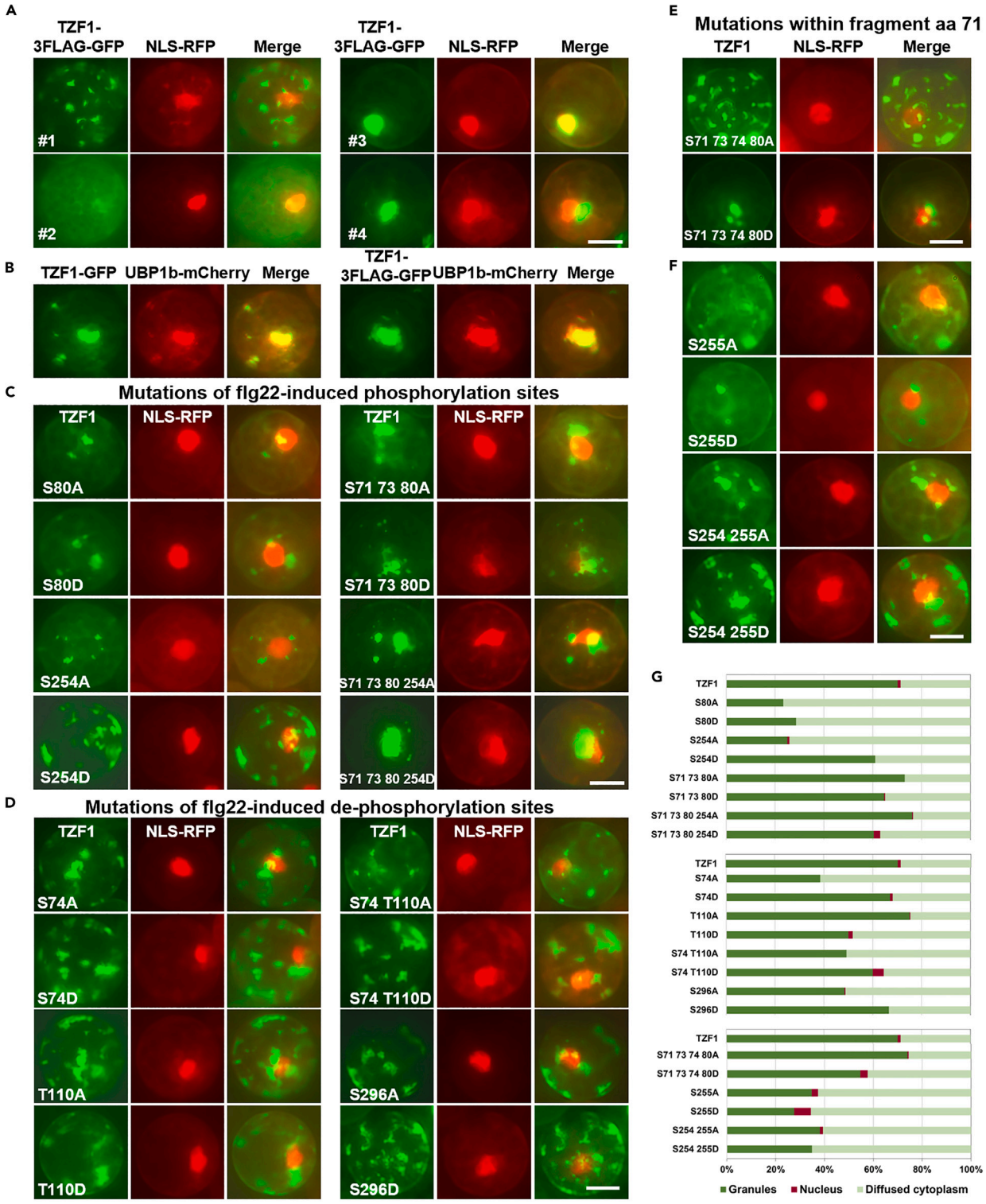

Figure 8. The effects of phosphorylation mutations on TZF1 cytoplasmic granule assembly

(A) TZF1-3FLAG-GFP fusion protein is mainly localized in cytoplasmic condensates/granules (#1) in Arabidopsis protoplasts. A small percentage of the cells display diffused cytoplasmic (#2), nuclear (#3), or nucleus-like (#4) patterns. NLS-RFP, a marker for nuclear proteins. Scale bar = 10 μm.

(B) TZF1 completely co-localized with SG marker UBP1b.

Figure 8. *Continued*

(C–F) The subcellular localization patterns of TZF1-3FLAG-GFP with mutations on the residues phosphorylated (C), de-phosphorylated (D) upon flg22 treatment, a fragment with compact flg22-induced phosphorylated (S71, S73, and S80) or dephosphorylated (S74) residues (E), and a predicted MAPK phosphorylation residue (S255) and S254/255 double mutation (F). The S to A change represents phosphor-dead and the S to D change represents phospho-mimicking mutation. Scale bar = 10 μm.

(G) Statistical analysis of TZF1-3FLAG-GFP subcellular localization patterns as shown in (A–F). Total number of cells counted $n > 250$ for each construct.

TZF1-OX plants (Figure 10C). Immunoblot analysis indicated that TZF1-GFP accumulated at a higher level in the WT than in the *keg-4* gain-of-function mutant[48,49] in either intact plants (Figure 10D) or in isolated protoplasts (Figure 10E). Furthermore, TZF1-GFP fluorescence signals were much stronger in the WT than in the *keg-4* in an Arabidopsis protoplast transient expression analysis (Figure 10F). Lastly, PYR41

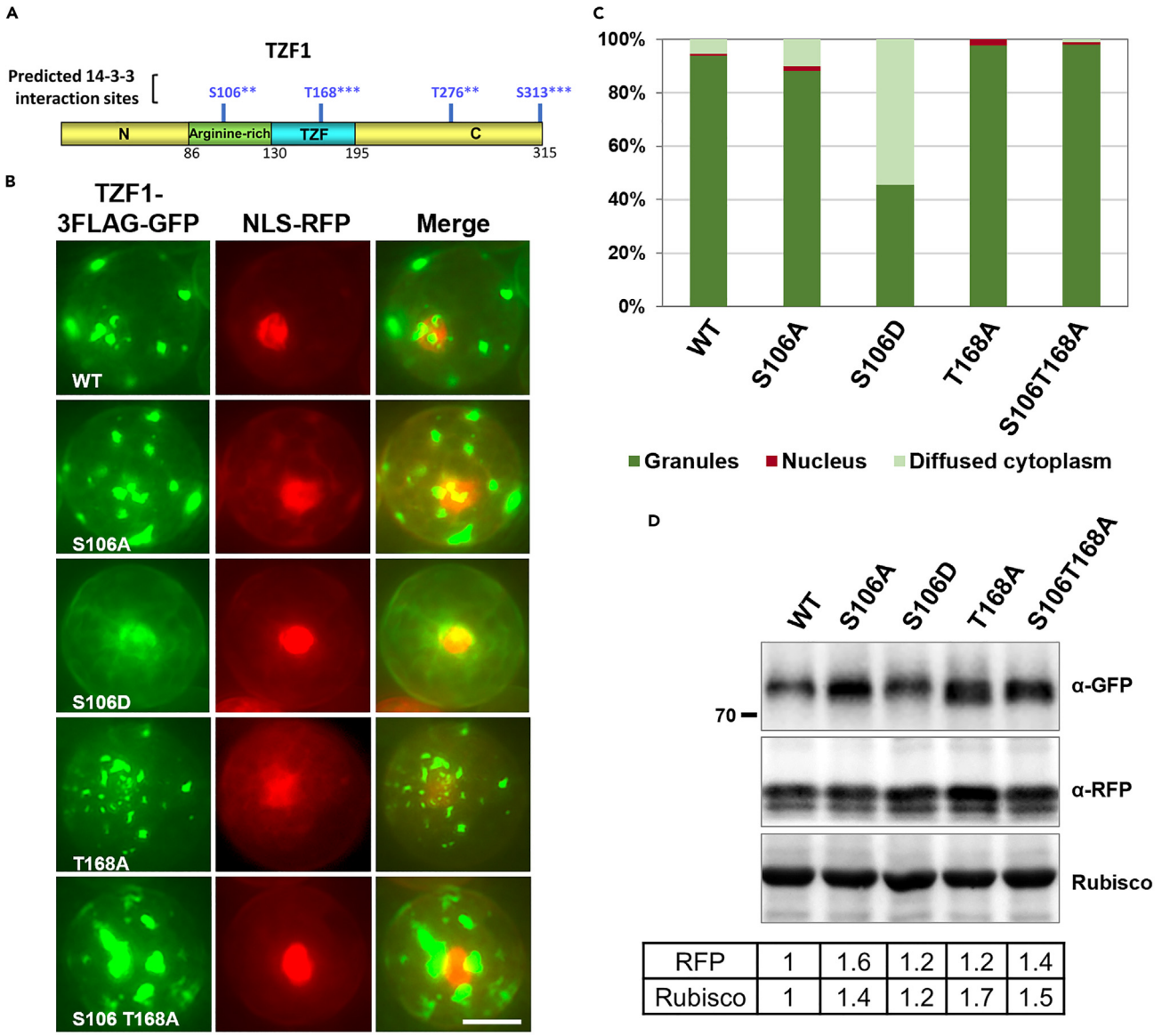

Figure 9. The effects of predicted 14-3-3 protein-protein interaction site mutations on TZF1 cytoplasmic granule assembly

(A) Four major 14-3-3 protein-protein interaction sites predicted by the 14-3-3-Pred algorithm (https://www.compbio.dundee.ac.uk/1433pred).

(B) Mutations (S/T to A) abolishing 14-3-3 interaction did not affect TZF1 localization to cytoplasmic granules, whereas S106D reduced cytoplasmic granule assembly. T168A appeared to enhance TZF1-GFP granule signal intensity. Scale bar = 10 μm.

(C) Statistical analysis of TZF1 subcellular localization patterns as shown in (B). Total number of cells counted $n > 250$ for each construct.

(D) Immunoblot analysis of TZF1 (WT) and 14-3-3 interaction site mutations. Numbers in the table indicate normalized values of GFP/RFP and GFP/Rubisco, respectively.

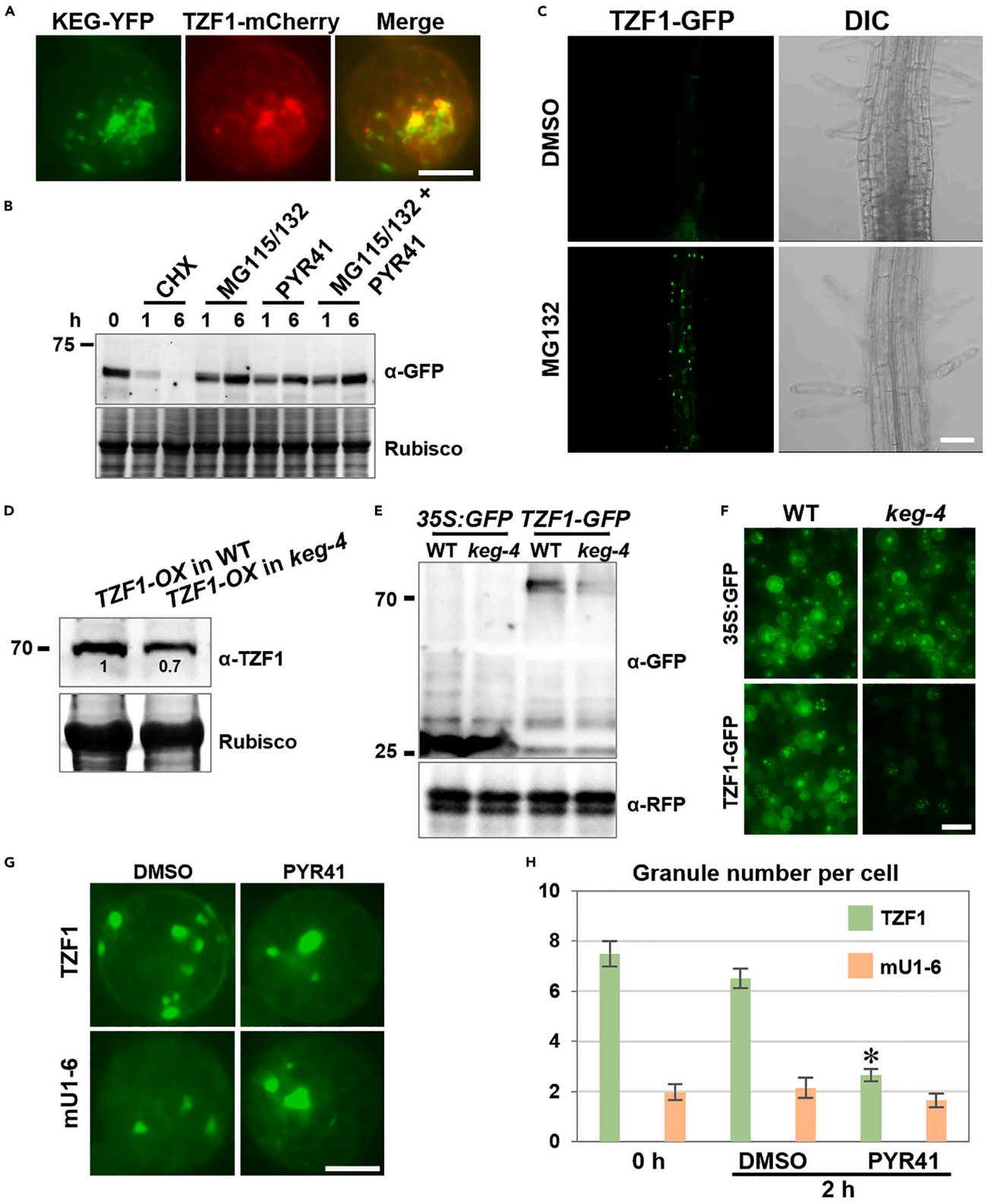
A
KEG-YFP
TZF1-mCherry
Merge
B
CHX
MG115/132
PYR41
MG115/132 + PYR41
h 0 1 6 1 6 1 6 1 6
75
α-GFP
Rubisco
C
TZF1-GFP
DIC
DMSO
MG132
D
TZF1-OX in WT
TZF1-OX in keg-4
70
1
0.7
α-TZF1
Rubisco
E
35S:GFP
TZF1-GFP
WT keg-4 WT keg-4
70
25
α-GFP
α-RFP
F
WT
keg-4
35S:GFP
TZF1-GFP
G
DMSO
PYR41
TZF1
mU1-6
H
Granule number per cell
TZF1
mU1-6
10
8
6
4
2
0
*
0 h
DMSO
PYR41
2 h

Figure 10. TZF1 accumulation is affected by KEG

(A) TZF1 is partially co-localized with KEG in cytoplasmic condensates. Scale bar = 10 μm.

(B) TZF1 accumulation was blocked by protein synthesis inhibitor CHX and enhanced by proteosome inhibitor MG115/132 cocktail in 7-day-old *TZF1-OX* transgenic plants.

(C) TZF1 cytoplasmic granules were enhanced by MG132 in the root cells of *TZF1-OX* transgenic plants. Scale bar = 20 mm.

(D) Immunoblot analysis indicated that TZF1-GFP accumulated at a higher level in the WT than in the *keg-4* gain-of-function mutant.

(E) Immunoblot analysis indicated that TZF1-GFP accumulated at a higher level in the WT than in the *keg-4* in Arabidopsis protoplasts.

(F) TZF1-GFP signals were much higher in the WT than in the *keg-4* in Arabidopsis protoplasts. Scale bar = 30 mm.

(G) TZF1 granule assembly was inhibited by PYR41. Scale bar = 10 μm.

(H) Quantitative analysis of granule number per cell as shown in (G). Columns represent means ± *SE* (*n* = 90). Asterisks indicate significant differences from 0 h (*, $p < 0.05$) by Student's t test.

inhibited SG assembly of TZF1(WT), but not the ubiquitination sites sextuple mutation (K to R change) TZF1$^{mU1\text{-}6}$ (Figures 10G, 10H, and 11A) due to inherited low number of SGs (described later). These results suggest that KEG might directly target TZF1 for ubiquitination-mediated degradation.

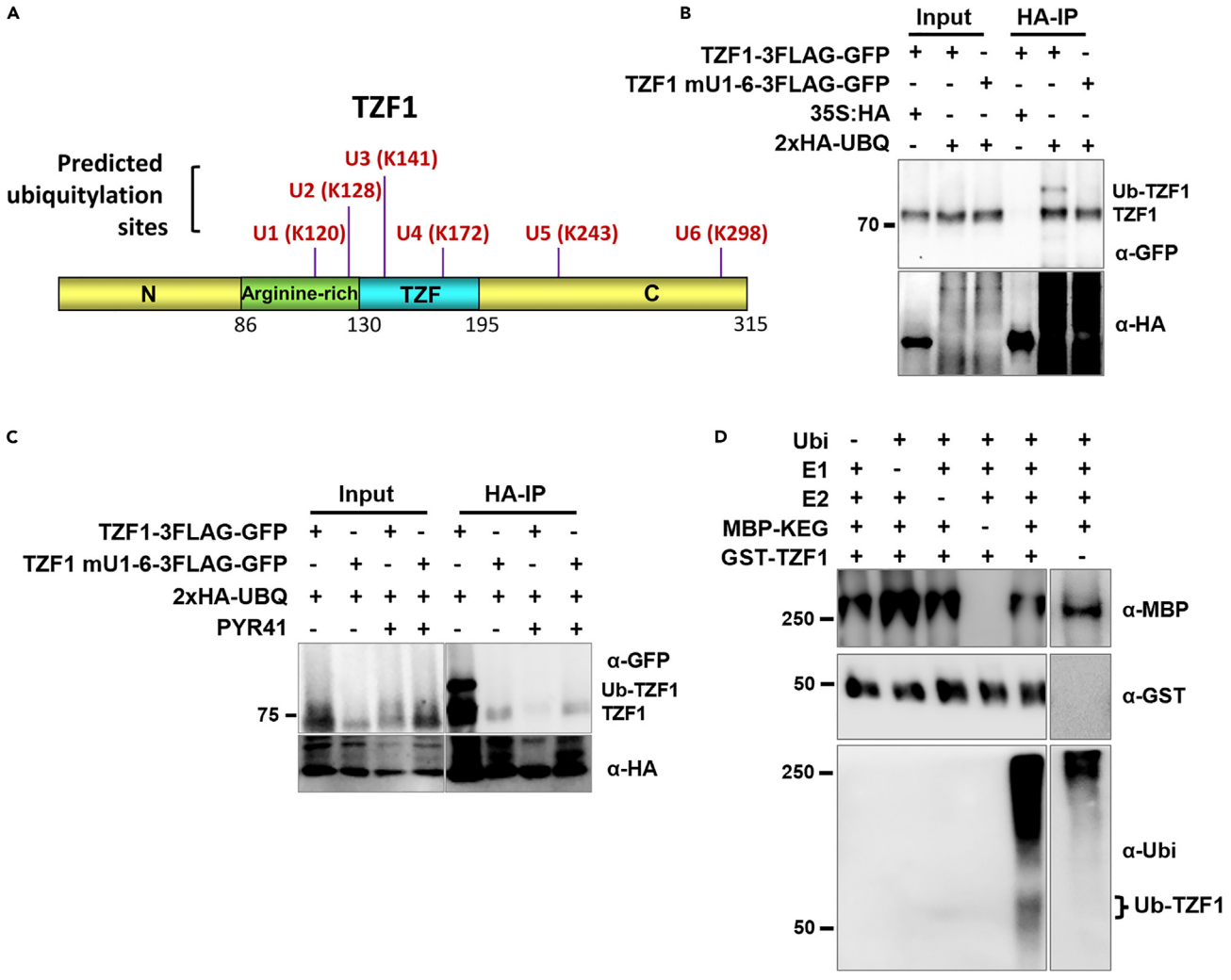

Figure 11. TZF1 is ubiquitinated *in vivo* and *in vitro*

(A) Schematic representation of ubiquitinated residues on TZF1 predicted by an online tool http://systbio.cau.edu.cn/araubisite.

(B) TZF1 is ubiquitinated *in vivo*. Arabidopsis protoplasts were co-expressed with indicated constructs and IP was performed using an anti-HA antibody and immunoblot was carried out using an anti-GFP antibody.

(C) Same IP experiment with the addition of ubiquitin-activating enzyme E1 inhibitor PYR41 was carried out.

(D) KEG ubiquitinates TZF1 *in vitro*. The *in vitro* reaction was carried out using recombinant E1, E2, and E3 (MBP-KEG) enzymes, ubiquitin, and GST-TZF1.

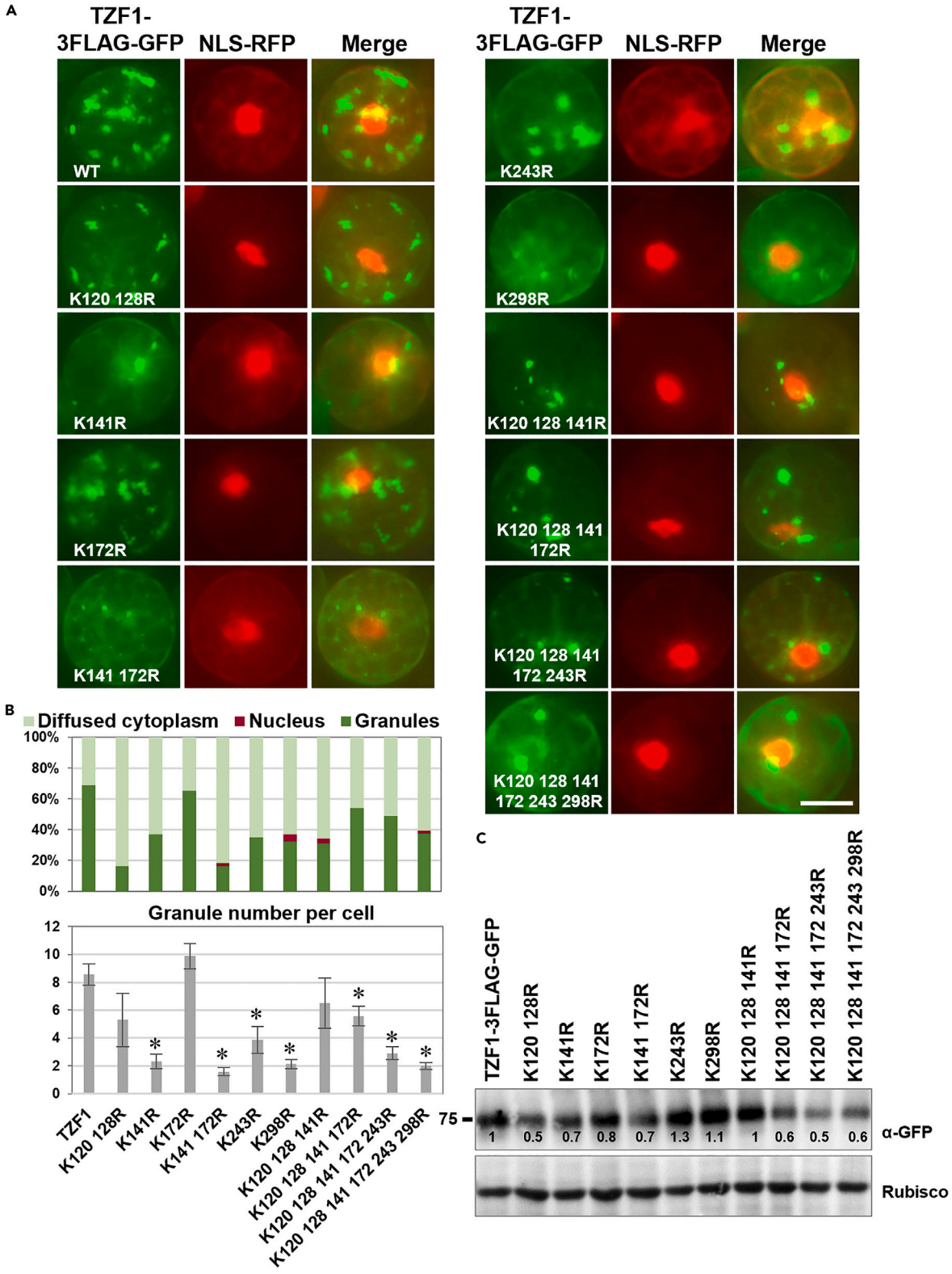
A
TZF1-3FLAG-GFP
NLS-RFP
Merge
WT
K120 128R
K141R
K172R
K141 172R
K243R
K298R
K120 128 141R
K120 128 141 172R
K120 128 141 172 243R
K120 128 141 172 243 298R
B
Diffused cytoplasm
Nucleus
Granules
100%
80%
60%
40%
20%
0%
Granule number per cell
12
10
8
6
4
2
0
TZF1
K120 128R
K141R
K172R
K141 172R
K243R
K298R
K120 128 141R
K120 128 141 172R
K120 128 141 172 243R
K120 128 141 172 243 298R
C
TZF1-3FLAG-GFP
K120 128R
K141R
K172R
K141 172R
K243R
K298R
K120 128 141R
K120 128 141 172R
K120 128 141 172 243R
K120 128 141 172 243 298R
75
1
0.5
0.7
0.8
0.7
1.3
1.1
1
0.6
0.5
0.6
α-GFP
Rubisco

Figure 12. The predicted ubiquitination site mutations abolished TZF1 stress granule assembly in Arabidopsis protoplasts

(A) All mutations appeared to reduce TZF1 stress granule assembly. Scale bar = 10 μm.

(B) Statistical analysis of TZF1 subcellular localization patterns and granule number per cell as shown in (A). Total number of cells counted $n > 250$ for each construct. Columns represent means ± *SE*. Asterisks indicate significant differences from TZF1 (*, $p < 0.05$) by Student's t test.

(C) Immunoblot analysis indicated that most ubiquitination site mutations reduced TZF1 protein accumulation.

TZF1 was predicted to contain six putative ubiquitination sites by AraUbiSite tool[62] (Figure 11A). To investigate whether TZF1 is a substrate of KEG, we performed *in vivo* and *in vitro* ubiquitination assays. HA-tagged ubiquitin (HA-Ub) was co-expressed with TZF1-3FLAG-GFP in wild-type Arabidopsis leaf protoplasts. Ubiquitinated proteins were purified by IP with anti-HA antibody coated beads and then revealed by immunoblot analysis with anti-HA or anti-GFP antibodies. Results showed that a potential ubiquitinated species was detected in TZF1, but not in the sextuple mutant $TZF1^{mU1\text{-}6}$ (Figure 11B). The same IP experiment with the addition of PYR41 was also carried out. While the potential ubiquitinated TZF1 band was reproducible, the sample with the addition of PYR41 was too weak to determine if TZF1 ubiquitination could be abolished by PYR41 (Figure 11C). Because KEG is strongly self-ubiquitinated[63] (Figure 11D), ubiquitination blocked by PYR41 would stabilize KEG, hence enhancing the degradation of TZF1. Next, we used recombinant GST-TZF1 and MBP-KEG (E3) to perform *in vitro* ubiquitination assays. High molecular-mass smear bands of TZF1 were detected in the presence of Ub, E1, and E2, and MBP-KEG (E3 ligase) enzymes. However, the reactions without GST-TZF1 or MBP-KEG failed to produce any detectable upper smear bands of GST-TZF1 (Figure 11D). Together, these results indicate that TZF1 is likely ubiquitinated by KEG.

Ubiquitination site mutations affect tandem CCCH zinc finger 1 stress granules assembly and protein-protein interaction with mitogen-activated kinase kinase 5

To determine if the ubiquitination of TZF1 affected SG assembly and protein-protein interaction with MKK5, site-directed mutagenesis was performed on predicted ubiquitination sites in TZF1. Intriguingly, except for $TZF1^{K172R}$, all single and higher order mutations caused a significant reduction of TZF1 SG assembly, particularly striking for $TZF1^{K120/128R}$ (within RR motif) and $TZF1^{K141R}$ and $TZF1^{K141/172R}$ (within TZF motif) mutants. It was noted that both the percentage of cells with granule pattern as well as granule number per cell were reduced, except for $TZF1^{K172R}$. Some large coalesced TZF1 SGs were observed in $TZF1^{K141R}$, $TZF1^{K243R}$, and quadruple and higher order mutants (Figures 12A and 12B), similar to the large SGs described earlier (Figures 8A and 8B). In addition, TZF1 ubiquitination site mutants still interacted with MKK5 in SGs. Except for $TZF1^{K120/128R}$, $TZF1^{K243R}$, $TZF1^{K120/128/141/172R}$, and $TZF1^{K120/128/141/172/243/298R}$, most mutations caused reduced interaction based on the decreased number of SGs (where TZF1 and MKK5 interacted) (Figure S9). It was even more clear that the ubiquitination site mutations appeared to cause coalescence of the condensates (where TZF1 and MKK5 interacted) that lacked clear boundaries. For TZF1 protein accumulation, mutations within the RR-TZF domain appeared to reduce TZF1 accumulation. These included $TZF1^{K120/128R}$, $TZF1^{K141R}$, $TZF1^{K172R}$, and $TZF1^{K141/172R}$, except for $TZF1^{K120/128/141R}$ with no effect on TZF1 accumulation. By contrast, mutations on the C-terminal domain ($TZF1^{K243R}$ and $TZF1^{K298R}$) caused higher levels of TZF1 accumulation, albeit not more than 30%. The higher order mutations (quadruple and up) caused a significant decrease in TZF1 accumulation, due to unknown reasons (Figure 12C). Together, these results suggest that mutations of TZF1 ubiquitination sites have much more pronounced effects on SG assembly than protein stability control, perhaps due to the involvement of other unknown factors and interactions.

DISCUSSION

Stress-induced RNP granules play pivotal roles in plant acclimation to various stresses and the class of SGs is conserved across different plant species.[2] RNP granules regulate gene expression at the post-transcriptional and translational levels. The assembly/disassembly of RNP granules is intimately controlled by intra- and extra-cellular cues via signal transduction mainly mediated by PTMs of key protein components such as RBPs. The PTMs involved include but are not limited to acetylation, arginine methylation, glycosylation, PARylation, phosphorylation, and ubiquitination.[64] In plants, our previous report revealed that flg22 could trigger the disassembly of PB component DCP1 granules in early immune response.[13] DCP1 is phosphorylated by MPK3/6 and the phosphorylation status dictates DCP1 granule assembly/disassembly as well as DCP1's role as a positive regulator in plant immune response. In this report, we have observed a parallel molecular mechanism that controls distinct roles of TZF1. TZF1 is mainly localized in SGs (Figure 3) and TZF1 is also phosphorylated by flg22-induced MAPK signaling cascade (Figure 6). However, in contrast to DCP1, TZF1 granules are induced by flg22 in the early phase (Figure 2) and TZF1 acts as a negative regulator in plant immune response (unpublished results). We therefore use the TZF1 SG assembly as a functional readout to systematically dissect the roles of various PTMs in this process. We have found that phosphorylation, ubiquitination, and 14-3-3 protein-protein interaction could all play pivotal roles in the modulation of TZF1 SG assembly/disassembly. We have also found that PTMs not only affect the formation/number but also the morphology of TZF1 SGs. We showed that $TZF1^{WT}$ (Figures S1D and 10C), other PB and SG markers (Figure 1), and signals of MKKs (Figure 5B), $TZF1^{WT}$-MPKs, and $TZF1^{WT}$-MKKs (Figures 4D and S3) displayed typical droplet-like RNP granule morphology. However, mutations that affected PTMs could change TZF1 SGs into aggregates-like larger SGs that were less typical. As plant SGs are not always droplet-like,[17,18,42,65,66] we propose that SG morphology can be modulated by external and internal cues and signal transduction mediated by PTMs.

Phosphorylation and ubiquitination in tristertraprolin model

TTP is one of the most highly phosphorylated proteins in animals. To date, nearly 50 phosphorylation sites have been identified in mouse mTTP (319 aa) and human hTTP (326 aa), respectively.[67] The stability and subcellular localization of TTP and its target mRNAs are tightly regulated by PTMs. The classical model of TTP-mRNA regulation is well established (Figure S10A)—in the unstimulated condition, TTP is localized in the nucleus and SGs in which both TTP and target mRNAs are labile. In the presence of proinflammatory stimulus, the $p38^{MAPK}$-MK2 pathway is activated to phosphorylate TTP at S52 and S178 outside of the TZF motif hence triggering 14-3-3 adaptor protein interaction. These events result in the exit of TTP from SGs to cytoplasm and the stabilization of both TTP and target mRNAs.[41,57]

With years of continuing research, layers of complexity have been added to this model (Figure S10A). The N-terminal domain of TTP is phosphorylated by an unusual kinase MEKK1 (MAP triple kinase 1) and then the MEKK1 binding partner E3 ubiquitin ligase TRAF2 (TNF receptor-associated factor 2) deposits K63-linked ubiquitin chains onto five lysine residues within central TZF motif. The progressive decrease of TTP phosphorylation and increase of ubiquitination leads to the reduction of Nuclear Factor-kappaB (NF-kB) activity (pro-cell survival), whereas the induction of the c-Jun N-terminal kinase (JNK) pathway (pro-cell death).[68] Curiously, the N-terminal domain of TTP also interacts with pyruvate kinase M2 (PKM2, typically a glycolysis enzyme) hence triggering $p38^{MAPK}$-MK2 mediated phosphorylation, ubiquitination of TTP, reduction of target mRNA turnover, and impairment of cell viability in breast cancer cells.[69]

In contrast to above mentioned non-degradative K63-mediated ubiquitination, TTP stability is also controlled by K48-mediated ubiquitination and degraded by 26S proteosome (Figure S10A). HECT, UBA, and WWE domain-containing protein 1 (HUWE1) is a giant E3 ubiquitin ligase that regulates numerous substrates involved in the signal transduction of cellular stress responses, cell growth, and apoptosis. A recent genetic analysis revealed that HUWE1 promotes the interaction between the TTP C-terminal domain (aa 234–259) and protein phosphatases PP1 and PP2 and inhibits $p38^{MAPK}$-MK2/JNK/ERK activities, therefore resulting in the dephosphorylation of TTP (within aa 259–279) and leading to an activation of an unknown E3 ligase to deposit K48 ubiquitin chains onto the TZF motif to destabilize TTP protein. This pathway represents the late phase (3–16 h) of the pro-inflammatory stimulus-induced response.[70]

Phosphorylation

Similar to that in animals,[1] plant SGs are formed via high local concentration and multivalent interaction of RNPs, where RBPs and signal transduction components such as kinases and phosphatases are enriched.[2] Kinase signaling has an intimate relationship with SGs—either the assembly of SGs is dependent on kinase signaling or certain kinases themselves contain IDRs that could act as scaffolds to mediate SG assembly. SGs could serve as hubs to sequester kinases, cofactors, and substrates to spatiotemporally facilitate kinase signaling on client proteins of SGs.[71] In plants, little is known about the roles of protein phosphorylation on the assembly of and protein-protein interaction within SGs. Although numerous reports have demonstrated the central roles of scaffold proteins and PTMs in nucleating and promoting SG assembly, none except G3PB-deficient mutants completely failed to form SGs in non-plant systems, and surprisingly the same phenomenon has not been observed in plant systems.[2]

In this report, we demonstrate the interaction and localization of MAPK signaling components in TZF1-associated SGs. These results are strongly supported by a previous protein interactome analysis indicating that MPK3, MKK4, and MKK5 were found in various SG proteomes.[2] We also unequivocally demonstrated that TZF1 is an IDR-containing SG component likely to play a key role in RNA metabolism and signal transduction.[72] Our study went a step further to show that MPKs and MKKs are recruited by TZF1 to SGs and TZF1 is phosphorylated by MPK3/6 (Figures 4, 5, and 6; Figures S3 and S5). The TZF1-MPK/MKK interaction in SGs is further substantiated by our IP-MS results in which conserved SG markers RH6/8/12 are also found in the TZF1 protein complex (Figure 4A). We then fine mapped the phosphorylation sites of the TZF1 using LC-MS/MS to reveal 10 potential residues, among which S80 and S254 are associated with MPK phosphorylation signature motif SP, and S106 and T276 are within predicted 14-3-3 adaptor protein binding sites (Figures 6 and 9A).

Our comprehensive mutant studies have revealed that phosphorylation has differential effects on TZF1 SG assembly and protein-protein interaction with MKK5 in SGs, depending on the location and phosphorylation status of the amino acids. As mentioned earlier, it was not surprising that none of the single or higher order mutations of either S to A or S to D changes could abolish SG assembly, given no prior examples could be found in plant systems. However, a significant reduction of SG assembly was found in the mutations of S80, and S254/255 (Figure 8), the two predicted MAPK phosphorylation sites. It is currently unclear though why both S to A and S to D changes resulted in similar SG reduction. We speculated that the phosphorylation status of these residues is tied to a feedback regulatory loop of SG homeostasis. Disruption of the balance of such loop controlled by reversible phosphorylation could lead to the disassembly of SGs (Figure 13).

Another striking result we have obtained is the relationship between phosphorylation and TZF1 protein accumulation. Although standard protein half-life analyses were not performed, the S to D mutations of almost all residues tested resulted in lower protein accumulation (Figure S6). This is in sharp contrast with the animal TTP model (Figure S10A) in which phosphorylated TTP is more stable.[41,57] Moving forward, it is imperative to unbiasedly determine and unravel the mechanism underpinning phosphorylation mediated control of TZF1 protein and target mRNAs stability.

14-3-3 adaptor protein interaction

The recruitment of 14-3-3 adaptor protein by MAPK signaling could have a significant impact on TZF1 function because 14-3-3 proteins could mask the IDRs of TZF1 and reduce its multivalency hence acting as inhibitors of TZF1-mediated SG assembly[71] (Figure S10). In this report, we confirm the role of IDR in SG assembly because the deletion of either or both IDRs in TZF1 almost eliminated SG assembly completely (Figures 3B and 3C). In addition, the deletion of IDRs from TZF1 also changed the pattern of protein-protein interaction with MKK5 from small

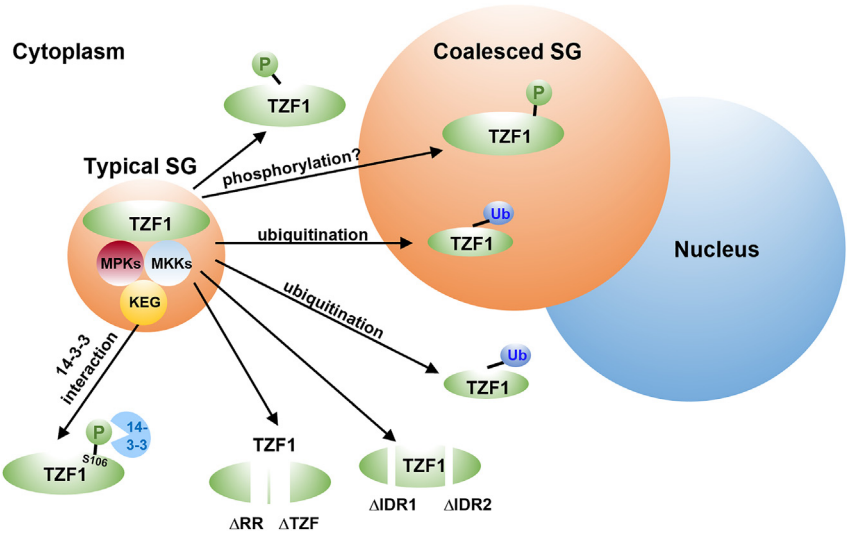

Figure 13. Effects of post-translational modifications on TZF1 SG assembly

Arabidopsis TZF1 recruits MAPK signaling components MPK3, MPK6, MKK4, and MKK5 and an E3 ubiquitin ligase KEG to SGs. TZF1 is phosphorylated by MPK3/6 and ubiquitinated by KEG. Depending on the position and status of the phosphorylation and ubiquitination modifications, TZF1 subcellular localization can be changed from a typical SG pattern to SG disassembly to become a cytoplasmic pattern or to the formation of one or more coalesced large SGs attaching to the nucleus. Deletion of IDR, RR, TZF motif, and phosphorylation-induced 14-3-3 interaction at TZF1 (S106) can also result in the reduction of SG assembly.

and even granular to a few large coalesced SGs near the nucleus (results not shown). This could be due to the compositional change in protein, RNA, or both in SGs. Furthermore, phosphorylation of a potential 14-3-3 interaction site (S106D) significantly reduced TZF1 SG assembly (Figure 9). Reduced SG assembly could be interpreted by the masking of TZF1's IDRs by 14-3-3 adaptor protein via phosphorylation dependent protein-protein interaction thus reducing TZF1's ability to recruit other components for SG assembly.

Ubiquitination

Ubiquitination is generally considered as a switch that destines protein for degradation by 26S proteosome. However, protein mono-ubiquitination and K63 type poly-ubiquitination are non-proteolytic signals that serve as means in controlling other cellular processes such as protein-protein interaction and protein phosphorylation, as have been intensively investigated in the NF-kB pathways. In animals, ubiquitination also regulates the activation of MAP kinases in immune and inflammatory pathways.[73] In another scenario, the K63-ubiquitination in the cells is required for DCP1a phosphorylation, decapping, and mRNA degradation of prototypical inflammatory genes, and most remarkably the assembly of decapping factors into PBs. Curiously, mutation of all six ubiquitin acceptor lysine residues (K520-577R) at the C-terminal of DCP1a increased the number but reduced the size of DCP1a-associated PBs, illustrating a multifaceted regulation of ubiquitination on the dynamics of PB assembly.[74]

Conversely, kinases could act as sensors for the PTM events taking place in LLPS-mediated condensates. For example, some kinases (e.g., TANK-binding kinase 1—TBK1) can sense ubiquitin and be recruited and activated (e.g., through oligomerization due to elevated local concentration) in the condensates enriched with ubiquitin-tagged misfolded proteins. This feedforward pathway can promote condensate growth and recruit additional polyubiquitin-tagged proteins to eventually trigger the participation of aggrephagy machinery (via TBK1 phosphorylation of aggrephagy receptors) to clear toxic protein aggregates that cause degenerative diseases such as amyotrophic lateral sclerosis (ALS).[71] In plants, an activator of salicylic acid induced systemic acquired resistance NPR1 (nonexpresser of PR genes 1) is recruited to the cellular condensates to trigger a partner E3 ubiquitin ligase mediated ubiquitination of other proteins in the condensates to enhance cell survival.[75]

In this report, we show that TZF1 is ubiquitinated by E3 ubiquitin ligase KEG (Figure 11). Intriguingly, mutations of predicted ubiquitination sites of TZF1 significantly reduce SG assembly and some mutations trigger the formation of large coalesced SGs in the proximity of the nucleus (Figure 12). It is well documented that RNP granules can undergo homotypic or heterotypic interaction to facilitate the assembly or larger granules. In general, SGs prefer to interact with themselves and two or more SGs can dock and form a larger condensate. By contrast, it is relatively rare for heterotypic docking of PBs with SGs to allow the exchange of RNPs including mRNAs.[1] We propose that TZF1 ubiquitination facilitates homotypic interaction via docking and merging to form larger SGs. However, we cannot rule out the possibility of heterotypic interaction, given that TZF1 could partially localize to PBs as well.[50] It is currently unclear whether the composition or property of TZF1 granules would be changed during the formation of a single or multiple aggregates-like large condensates within the cells (Figure 8A). As was reported recently, RNAs were primarily degraded in smaller liquid-like PBs, whereas RNAs were mostly stable under heat shock conditions when PBs increased in size and became more solid-like.[76] In our study, we do not know the properties, composition, and fate of the RNAs associated with TZF1 condensates, but we do observe in numerous occasions the dynamic changes of the size and number of TZF1

condensates among various mutations (Figure 13), implicating that PTM such as phosphorylation and ubiquitination might affect TZF1 condensates' ability in modulating mRNA metabolism.

On the other hand, it is currently unclear how the large TZF1 SGs are connected to the nucleus. Perinuclear RNA granules such as germ granules (known as P granules in Caenorhabditis elegans) are well characterized to be associated with nuclear pore complex (NPC).[77] However, there could be up to a dozen of P granules surrounding a single nucleus, which is quite different from what we have observed here that which only a single or a couple of TZF1 SGs are present. Nevertheless, it was demonstrated recently that the NPC proxiome assembly is mediated by phase separation in plants. For example, PBs can be directly associated with NPCs to regulate translation and mRNA stability.[78] There are also multiple reports that support the notion of the component-exchange cycle between PBs and SGs.[2] We propose that TZF1 could play a role in modulating SG-nucleus material exchange cycle and/or function-coupling. The cause and biological significance of large coalesced SGs near the nucleus are important questions to be addressed in the future.

Another striking result in our study is the reduction of TZF1 protein accumulation resulting from mutations of ubiquitination sites (Figure 12C). We do not know if TZF1 is ubiquitinated via K48 or K63 or both ubiquitin chains. Given the results of immunoblot analysis we have obtained, it might be more likely that TZF1 is predominantly K63-ubiquitinated. Mutagenesis of ubiquitination sites is frequently used to validate ubiquitination targets. However, the results from using this approach can be difficult to interpret due to unintended changes in protein folding, protein-protein interaction, ATP/ubiquitin binding, and protein activities.[73] Therefore, reduced TZF1 accumulation caused by ubiquitination site mutations could be a consequence of multiple reasons mentioned above. A deeper dissection of the mechanisms of TZF1 ubiquitination is required to address these important open questions in the future.

Limitations of the study

In this report, various analyses were conducted using both intact plants and protoplasts. Although the protoplast transient expression system was highly efficient and versatile,[53] it could present some potential problems. The use of the protoplast system was meant to be a reductionist approach in which artifacts might exist, but the major focus was to compare the phenotypes between the WT and the mutant proteins. Nevertheless, leaf protoplasts are mainly derived from mesophyll cells that have very different cell geometries compared to the uniform spherical protoplasts. The viscoelastic properties of a biomolecular condensate such as SG determine its interaction with other molecules in the cells and the shape of the biomolecular condensates. The interacting molecules could be materials in the cytoplasm or nucleoplasm, chromatin, cytoskeleton, microtubules, and various membranes. The viscoelasticity of the interacting materials also affects biomolecular condensates geometries and vice versa.[79] The extent of the changes in cellular contents, due to the alteration of cell geometry from intact leaf mesophyll cells to protoplasts has not been documented. However, it is conceivable that the two would not be identical. It was reported recently that DCP1 protein condensates interact with plasma membranes and are differentially accumulated at the edges and vertices of root cells in different regions.[60] Such specific subcellular localization patterns could not have been observed in the root protoplasts.

Another potential drawback of our studies was the use of the *CaMV35S* promoter to drive the reporter gene expression to a high level. Again, the use of the *CaMV35S* promoter was meant to boost the protein expression to enlarge the scale of the difference between WT and mutant proteins. Although one could argue that biomolecular condensate formation is primarily a post-translational event. The crowding of the scaffold proteins could significantly enhance phase-separation hence increasing the number and perhaps the size of the condensates.[80] For example, compared to MKK4 and MKK5, MPK3 and MPK6 cannot be expressed to a comparable high level even when driven by *CaMV35S* promoter. Perhaps due to this reason, MPK3 and MPK6 were rarely seen localized to the condensates (Figure 5A). However, one could also argue that perhaps there is indeed a difference between MPK3/6 and MKK4/5, because MPK3/6 could readily be localized to the condensates when co-expressed with TZF1, but not a nuclear marker NLS-RFP (Figure 5C). Whether or not the crowding of TZF1 recruits MPK3/6 to SGs awaits future analysis using intact transgenic plants and placing these reporter constructs under the native promoter with an inducible switch.

Conclusion

In summary, we have found that TZF1 recruits MAPK signaling components and an E3 ubiquitin ligase KEG to SGs (Figure 13). TZF1 is then phosphorylated by MPKs and ubiquitinated by KEG. In this process, we have found that Arabidopsis TZF1 is not less complicated than animal TTP, in terms of domain/structure and function (Figure S10A). Phosphorylation, ubiquitination, 14-3-3 interaction, IDRs, and numerous regulatory elements throughout TZF1 might all have differential effects on RNP granule assembly and protein-protein interaction with a key MAPK signaling component MKK5 in SGs (Figure 13). Given decades of intensive studies on mammalian TTP, our understanding of Arabidopsis TZF1 thus far appears to be in its infancy and one-dimensional (Figure S10B). However, we believe our groundbreaking study has served as a gateway for more intensive investigation in the future. Moving forward, in-depth characterization of these transgenic plants is expected to gain more insights into plant SG dynamics in response to various cues. Because TZF family proteins are evolutionarily conserved not only in sequence and structure but also in expression pattern and function, much more work is required to translate basic information into useful new tools for potential crop improvement.

RESOURCE AVAILABILITY

Lead contact

Further information and requests for resources and reagents should be directed to and will be fulfilled by the lead contact, Dr. Jyan-Chyun Jang (jang.40@osu.edu).

Materials availability

This study did not generate new unique reagents.

Data and code availability

- All data reported in this article will be shared by the lead contact upon request.
- This article does not report the original code.
- Any additional information required to reanalyze the data reported in this article is available from the lead contact upon request.

ACKNOWLEDGMENTS

We thank Dr. Roger W. Innes (Department of Biology, Indiana University, Bloomington, Indiana) for providing the KEG-YFP plasmid and Dr. Geng-Jen Jang and Hsuan Pai for providing a graphical abstract.

Funding sources: This work was supported by the grants from National Science Foundation MCB-1906060 to J.C. Jang, P. He, L. Shan, and Y. Wang; Ohio State University President's Research Excellence Accelerator award, Ohio Agricultural Research and Development Center SEEDS Program #2018007, Ohio State University College of Food, Agricultural, and Environmental Sciences Internal Grant Program #2022014, and Ohio State University Center for Applied Plant Sciences Research Enhancement Grant to J.C. Jang; National Natural Science Foundation of China (No. 32370307) to L. Wang.

AUTHOR CONTRIBUTIONS

Conceptualization, S.L.H. and J.C.J.; methodology, S.L.H. and J.C.J; investigation, S.L.H., X.W., A.L., and L.K.; resources, S.I.K. and L.K.; visualization, S.L.H., J.C.J., X.W., and L.K., supervision, J.C.J., L.W., P.H., L.S., and Y.W.; writing – original draft, S.L.H. and J.C.J; writing – review and editing, S.L.H., J.C.J., L.W., P.H., L.S., Y.W.; funding acquisition, J.C.J., L.W., P.H., L.S., and Y.W.

DECLARATION OF INTERESTS

The authors declare no competing interests.

STAR★METHODS

Detailed methods are provided in the online version of this paper and include the following:

SUPPLEMENTAL INFORMATION

Supplemental information can be found online at https://doi.org/10.1016/j.isci.2024.111162.

Received: July 13, 2024
Revised: October 8, 2024
Accepted: October 9, 2024
Published: October 23, 2024

REFERENCES

1. Ripin, N., and Parker, R. (2023). Formation, function, and pathology of RNP granules. Cell *186*, 4737–4756. https://doi.org/10.1016/j.cell.2023.09.006.
2. Solis-Miranda, J., Chodasiewicz, M., Skirycz, A., Fernie, A.R., Moschou, P.N., Bozhkov, P.V., and Gutierrez-Beltran, E. (2023). Stress-related biomolecular condensates in plants. Plant Cell *35*, 3187–3204. https://doi.org/10.1093/plcell/koad127.
3. Guzikowski, A.R., Chen, Y.S., and Zid, B.M. (2019). Stress-induced mRNP granules: Form and function of processing bodies and stress granules. Wiley Interdiscip. Rev. RNA *10*, e1524. https://doi.org/10.1002/wrna.1524.
4. Nostramo, R., Xing, S., Zhang, B., and Herman, P.K. (2019). Insights into the Role of P-Bodies and Stress Granules in Protein Quality Control. Genetics *213*, 251–265. https://doi.org/10.1534/genetics.119.302376.
5. Riggs, C.L., Kedersha, N., Ivanov, P., and Anderson, P. (2020). Mammalian stress granules and P bodies at a glance. J. Cell Sci. *133*, jcs242487. https://doi.org/10.1242/jcs.242487.
6. Decker, C.J., and Parker, R. (2012). P-bodies and stress granules: possible roles in the control of translation and mRNA degradation. Cold Spring Harb. Perspect. Biol. *4*, a012286. https://doi.org/10.1101/cshperspect.a012286.
7. Ivanov, P., Kedersha, N., and Anderson, P. (2019). Stress Granules and Processing Bodies in Translational Control. Cold Spring Harb. Perspect. Biol. *11*, a032813. https://doi.org/10.1101/cshperspect.a032813.
8. Kedersha, N., and Anderson, P. (2009). Regulation of translation by stress granules and processing bodies. Prog. Mol. Biol. Transl. Sci. *90*, 155–185. https://doi.org/10.1016/S1877-1173(09)90004-7.
9. Kedersha, N., and Anderson, P. (2007). Mammalian stress granules and processing bodies. Methods Enzymol.

431, 61–81. https://doi.org/10.1016/S0076-6879(07)31005-7.
10. Buchan, J.R., and Parker, R. (2009). Eukaryotic stress granules: the ins and outs of translation. Mol. Cell *36*, 932–941. https://doi.org/10.1016/j.molcel.2009.11.020.
11. Luo, Y., Na, Z., and Slavoff, S.A. (2018). P-Bodies: Composition, Properties, and Functions. Biochemistry *57*, 2424–2431. https://doi.org/10.1021/acs.biochem.7b01162.
12. Xu, J., and Chua, N.H. (2011). Processing bodies and plant development. Curr. Opin. Plant Biol. *14*, 88–93. https://doi.org/10.1016/j.pbi.2010.10.003.
13. Yu, X., Li, B., Jang, G.J., Jiang, S., Jiang, D., Jang, J.C., Wu, S.H., Shan, L., and He, P. (2019). Orchestration of Processing Body Dynamics and mRNA Decay in Arabidopsis Immunity. Cell Rep. *28*, 2194–2205.e6. https://doi.org/10.1016/j.celrep.2019.07.054.
14. Xu, J., and Chua, N.H. (2012). Dehydration stress activates Arabidopsis MPK6 to signal DCP1 phosphorylation. EMBO J. *31*, 1975–1984. https://doi.org/10.1038/emboj.2012.56.
15. Protter, D.S.W., and Parker, R. (2016). Principles and Properties of Stress Granules. Trends Cell Biol. *26*, 668–679. https://doi.org/10.1016/j.tcb.2016.05.004.
16. Campos-Melo, D., Hawley, Z.C.E., Droppelmann, C.A., and Strong, M.J. (2021). The Integral Role of RNA in Stress Granule Formation and Function. Front. Cell Dev. Biol. *9*, 621779. https://doi.org/10.3389/fcell.2021.621779.
17. Gutierrez-Beltran, E., Moschou, P.N., Smertenko, A.P., and Bozhkov, P.V. (2015). Tudor staphylococcal nuclease links formation of stress granules and processing bodies with mRNA catabolism in Arabidopsis. Plant Cell *27*, 926–943. https://doi.org/10.1105/tpc.114.134494.
18. Weber, C., Nover, L., and Fauth, M. (2008). Plant stress granules and mRNA processing bodies are distinct from heat stress granules. Plant J. *56*, 517–530. https://doi.org/10.1111/j.1365-313X.2008.03623.x.
19. Nguyen, C.C., Nakaminami, K., Matsui, A., Kobayashi, S., Kurihara, Y., Toyooka, K., Tanaka, M., and Seki, M. (2016). Oligouridylate Binding Protein 1b Plays an Integral Role in Plant Heat Stress Tolerance. Front. Plant Sci. *7*, 853. https://doi.org/10.3389/fpls.2016.00853.
20. Bogamuwa, S.P., and Jang, J.C. (2014). Tandem CCCH zinc finger proteins in plant growth, development and stress response. Plant Cell Physiol. *55*, 1367–1375. https://doi.org/10.1093/pcp/pcu074.
21. Blackshear, P.J., Phillips, R.S., and Lai, W.S. (2005). Tandem CCCH Zinc Finger Proteins in mRNA Binding. In Zinc Finger Proteins: From Atomic Contact to Cellular Function, S. Iuchi and N. Kuldell, eds. (Springer US), pp. 80–90. https://doi.org/10.1007/0-387-27421-9_13.
22. Chai, G., Hu, R., Zhang, D., Qi, G., Zuo, R., Cao, Y., Chen, P., Kong, Y., and Zhou, G. (2012). Comprehensive analysis of CCCH zinc finger family in poplar (Populus trichocarpa). BMC Genom. *13*, 253. https://doi.org/10.1186/1471-2164-13-253.
23. Jang, J.C. (2016). Arginine-rich motif-tandem CCCH zinc finger proteins in plant stress responses and post-transcriptional regulation of gene expression. Plant Sci. *252*, 118–124. https://doi.org/10.1016/j.plantsci.2016.06.014.
24. Peng, X., Zhao, Y., Cao, J., Zhang, W., Jiang, H., Li, X., Ma, Q., Zhu, S., and Cheng, B. (2012). CCCH-type zinc finger family in maize: genome-wide identification, classification and expression profiling under abscisic acid and drought treatments. PLoS One *7*, e40120. https://doi.org/10.1371/journal.pone.0040120.
25. Wang, D., Guo, Y., Wu, C., Yang, G., Li, Y., and Zheng, C. (2008). Genome-wide analysis of CCCH zinc finger family in Arabidopsis and rice. BMC Genom. *9*, 44. https://doi.org/10.1186/1471-2164-9-44.
26. Xu, R. (2014). Genome-wide analysis and identification of stress-responsive genes of the CCCH zinc finger family in Solanum lycopersicum. Mol. Genet. Genomics. *289*, 965–979. https://doi.org/10.1007/s00438-014-0861-1.
27. Kong, Z., Li, M., Yang, W., Xu, W., and Xue, Y. (2006). A novel nuclear-localized CCCH-type zinc finger protein, OsDOS, is involved in delaying leaf senescence in rice. Plant Physiol. *141*, 1376–1388.
28. Jan, A., Maruyama, K., Todaka, D., Kidokoro, S., Abo, M., Yoshimura, E., Shinozaki, K., Nakashima, K., and Yamaguchi-Shinozaki, K. (2013). OsTZF1, a CCCH-tandem zinc finger protein, confers delayed senescence and stress tolerance in rice by regulating stress-related genes. Plant Physiol. *161*, 1202–1216. https://doi.org/10.1104/pp.112.205385.
29. Lin, P.C., Pomeranz, M.C., Jikumaru, Y., Kang, S.G., Hah, C., Fujioka, S., Kamiya, Y., and Jang, J.C. (2011). The Arabidopsis tandem zinc finger protein AtTZF1 affects ABA- and GA-mediated growth, stress and gene expression responses. Plant J. *65*, 253–268. https://doi.org/10.1111/j.1365-313X.2010.04419.x.
30. Bogamuwa, S., and Jang, J.C. (2013). The Arabidopsis tandem CCCH zinc finger proteins AtTZF4, 5 and 6 are involved in light-, abscisic acid- and gibberellic acid-mediated regulation of seed germination. Plant Cell Environ. *36*, 1507–1519. https://doi.org/10.1111/pce.12084.
31. Chao, Y., Zhang, T., Yang, Q., Kang, J., Sun, Y., Gruber, M.Y., and Qin, Z. (2014). Expression of the alfalfa CCCH-type zinc finger protein gene MsZFN delays flowering time in transgenic Arabidopsis thaliana. Plant Sci. *215–216*, 92–99. https://doi.org/10.1016/j.plantsci.2013.10.012.
32. Anderson, P., and Kedersha, N. (2009). RNA granules: post-transcriptional and epigenetic modulators of gene expression. Nat. Rev. Mol. Cell Biol. *10*, 430–436. https://doi.org/10.1038/nrm2694.
33. Carballo, E., Lai, W.S., and Blackshear, P.J. (1998). Feedback inhibition of macrophage tumor necrosis factor-alpha production by tristetraprolin. Science *281*, 1001–1005.
34. Lai, W.S., Carballo, E., Strum, J.R., Kennington, E.A., Phillips, R.S., and Blackshear, P.J. (1999). Evidence that tristetraprolin binds to AU-rich elements and promotes the deadenylation and destabilization of tumor necrosis factor alpha mRNA. Mol. Cell Biol. *19*, 4311–4323.
35. Guo, C., Chen, L., Cui, Y., Tang, M., Guo, Y., Yi, Y., Li, Y., Liu, L., and Chen, L. (2022). RNA Binding Protein OsTZF7 Traffics Between the Nucleus and Processing Bodies/Stress Granules and Positively Regulates Drought Stress in Rice. Front. Plant Sci. *13*, 802337. https://doi.org/10.3389/fpls.2022.802337.
36. Seong, S.Y., Shim, J.S., Bang, S.W., and Kim, J.K. (2020). Overexpression of OsC3H10, a CCCH-Zinc Finger, Improves Drought Tolerance in Rice by Regulating Stress-Related Genes. Plants *9*, 1298. https://doi.org/10.3390/plants9101298.
37. Li, B., Wang, Y., Zhang, Y., Tian, W., Chong, K., Jang, J.C., and Wang, L. (2019). PRR5, 7 and 9 positively modulate TOR signaling-mediated root cell proliferation by repressing TANDEM ZINC FINGER 1 in Arabidopsis. Nucleic Acids Res. *47*, 5001–5015. https://doi.org/10.1093/nar/gkz191.
38. Owen, I., and Shewmaker, F. (2019). The Role of Post-Translational Modifications in the Phase Transitions of Intrinsically Disordered Proteins. Int. J. Mol. Sci. *20*, 5501. https://doi.org/10.3390/ijms20215501.
39. Millar, S.R., Huang, J.Q., Schreiber, K.J., Tsai, Y.C., Won, J., Zhang, J., Moses, A.M., and Youn, J.Y. (2023). A New Phase of Networking: The Molecular Composition and Regulatory Dynamics of Mammalian Stress Granules. Chem. Rev. *123*, 9036–9064. https://doi.org/10.1021/acs.chemrev.2c00608.
40. Ohn, T., and Anderson, P. (2010). The role of posttranslational modifications in the assembly of stress granules. Wiley Interdiscip. Rev. RNA *1*, 486–493. https://doi.org/10.1002/wrna.23.
41. Stoecklin, G., Stubbs, T., Kedersha, N., Wax, S., Rigby, W.F.C., Blackwell, T.K., and Anderson, P. (2004). MK2-induced tristetraprolin:14-3-3 complexes prevent stress granule association and ARE-mRNA decay. EMBO J. *23*, 1313–1324.
42. Tabassum, N., Eschen-Lippold, L., Athmer, B., Baruah, M., Brode, M., Maldonado-Bonilla, L.D., Hoehenwarter, W., Hause, G., Scheel, D., and Lee, J. (2020). Phosphorylation-dependent control of an RNA granule-localized protein that fine-tunes defence gene expression at a post-transcriptional level. Plant J. *101*, 1023–1039. https://doi.org/10.1111/tpj.14573.
43. Krause, L.J., Herrera, M.G., and Winklhofer, K.F. (2022). The Role of Ubiquitin in Regulating Stress Granule Dynamics. Front. Physiol. *13*, 910759. https://doi.org/10.3389/fphys.2022.910759.
44. Tolay, N., and Buchberger, A. (2022). Role of the Ubiquitin System in Stress Granule Metabolism. Int. J. Mol. Sci. *23*, 3624. https://doi.org/10.3390/ijms23073624.
45. Gwon, Y., Maxwell, B.A., Kolaitis, R.M., Zhang, P., Kim, H.J., and Taylor, J.P. (2021). Ubiquitination of G3BP1 mediates stress granule disassembly in a context-specific manner. Science *372*, eabf6548. https://doi.org/10.1126/science.abf6548.
46. Alexander, E.J., Ghanbari Niaki, A., Zhang, T., Sarkar, J., Liu, Y., Nirujogi, R.S., Pandey, A., Myong, S., and Wang, J. (2018). Ubiquilin 2 modulates ALS/FTD-linked FUS-RNA complex dynamics and stress granule formation. Proc. Natl. Acad. Sci. USA *115*, E11485–E11494. https://doi.org/10.1073/pnas.1811997115.
47. Huang, C., Chen, Y., Dai, H., Zhang, H., Xie, M., Zhang, H., Chen, F., Kang, X., Bai, X., and Chen, Z. (2020). UBAP2L arginine methylation by PRMT1 modulates stress granule assembly. Cell Death Differ. *27*, 227–241. https://doi.org/10.1038/s41418-019-0350-5.
48. Gao, C., Sun, P., Wang, W., and Tang, D. (2021). Arabidopsis E3 ligase KEG associates with and ubiquitinates MKK4 and MKK5 to regulate plant immunity. J. Integr. Plant Biol. *63*, 327–339. https://doi.org/10.1111/jipb.13007.

49. Wawrzynska, A., Christiansen, K.M., Lan, Y., Rodibaugh, N.L., and Innes, R.W. (2008). Powdery mildew resistance conferred by loss of the ENHANCED DISEASE RESISTANCE1 protein kinase is suppressed by a missense mutation in KEEP ON GOING, a regulator of abscisic acid signaling. Plant Physiol. *148*, 1510–1522. https://doi.org/10.1104/pp.108.127605.
50. Pomeranz, M.C., Hah, C., Lin, P.C., Kang, S.G., Finer, J.J., Blackshear, P.J., and Jang, J.C. (2010). The Arabidopsis tandem zinc finger protein AtTZF1 traffics between the nucleus and cytoplasmic foci and binds both DNA and RNA. Plant Physiol. *152*, 151–165. https://doi.org/10.1104/pp.109.145656.
51. He, S.L., Li, B., Zahurancik, W.J., Arthur, H.C., Sidharthan, V., Gopalan, V., Wang, L., and Jang, J.C. (2024). Overexpression of stress granule protein TZF1 enhances salt stress tolerance by targeting ACA11 mRNA for degradation in Arabidopsis. Front. Plant Sci. *15*, 1375478. https://doi.org/10.3389/fpls.2024.1375478.
52. Wu, F.H., Shen, S.C., Lee, L.Y., Lee, S.H., Chan, M.T., and Lin, C.S. (2009). Tape-Arabidopsis Sandwich - a simpler Arabidopsis protoplast isolation method. Plant Methods *5*, 16. https://doi.org/10.1186/1746-4811-5-16.
53. Sheen, J. (2001). Signal transduction in maize and Arabidopsis mesophyll protoplasts. Plant Physiol. *127*, 1466–1475.
54. Liu, C., Mentzelopoulou, A., Hatzianestis, I.H., Tzagkarakis, E., Skaltsogiannis, V., Ma, X., Michalopoulou, V.A., Romero-Campero, F.J., Romero-Losada, A.B., Sarris, P.F., et al. (2024). A proxitome-RNA-capture approach reveals that processing bodies repress coregulated hub genes. Plant Cell *36*, 559–584. https://doi.org/10.1093/plcell/koad288.
55. Qu, J., Kang, S.G., Wang, W., Musier-Forsyth, K., and Jang, J.C. (2014). The Arabidopsis thaliana tandem zinc finger 1 (AtTZF1) protein in RNA binding and decay. Plant J. *78*, 452–467. https://doi.org/10.1111/tpj.12485.
56. Cao, H., Deterding, L.J., Venable, J.D., Kennington, E.A., Yates, J.R., 3rd, Tomer, K.B., and Blackshear, P.J. (2006). Identification of the anti-inflammatory protein tristetraprolin as a hyperphosphorylated protein by mass spectrometry and site-directed mutagenesis. Biochem. J. *394*, 285–297.
57. Sandler, H., and Stoecklin, G. (2008). Control of mRNA decay by phosphorylation of tristetraprolin. Biochem. Soc. Trans. *36*, 491–496. https://doi.org/10.1042/BST0360491.
58. Mahtani, K.R., Brook, M., Dean, J.L., Sully, G., Saklatvala, J., and Clark, A.R. (2001). Mitogen-activated protein kinase p38 controls the expression and posttranslational modification of tristetraprolin, a regulator of tumor necrosis factor alpha mRNA stability. Mol. Cell Biol. *21*, 6461–6469. https://doi.org/10.1128/MCB.21.9.6461-6469.2001.
59. Powers, S.K., Holehouse, A.S., Korasick, D.A., Schreiber, K.H., Clark, N.M., Jing, H., Emenecker, R., Han, S., Tycksen, E., Hwang, I., et al. (2019). Nucleo-cytoplasmic Partitioning of ARF Proteins Controls Auxin Responses in Arabidopsis thaliana. Mol. Cell *76*, 177–190.e5. https://doi.org/10.1016/j.molcel.2019.06.044.
60. Liu, C., Mentzelopoulou, A., Muhammad, A., Volkov, A., Weijers, D., Gutierrez-Beltran, E., and Moschou, P.N. (2023). An actin remodeling role for Arabidopsis processing bodies revealed by their proximity interactome. EMBO J. *42*, e111885. https://doi.org/10.15252/embj.2022111885.
61. Gu, Y., and Innes, R.W. (2012). The KEEP ON GOING protein of Arabidopsis regulates intracellular protein trafficking and is degraded during fungal infection. Plant Cell *24*, 4717–4730. https://doi.org/10.1105/tpc.112.105254.
62. Wang, X., Yan, R., Chen, Y.Z., and Wang, Y. (2021). Computational identification of ubiquitination sites in Arabidopsis thaliana using convolutional neural networks. Plant Mol. Biol. *105*, 601–610. https://doi.org/10.1007/s11103-020-01112-w.
63. Liu, H., and Stone, S.L. (2010). Abscisic acid increases Arabidopsis ABI5 transcription factor levels by promoting KEG E3 ligase self-ubiquitination and proteasomal degradation. Plant Cell *22*, 2630–2641. https://doi.org/10.1105/tpc.110.076075.
64. Jeon, P., Ham, H.J., Park, S., and Lee, J.A. (2022). Regulation of Cellular Ribonucleoprotein Granules: From Assembly to Degradation via Post-translational Modification. Cells *11*, 2063. https://doi.org/10.3390/cells11132063.
65. Gutierrez-Beltran, E., Elander, P.H., Dalman, K., Dayhoff, G.W., Moschou, P.N., Uversky, V.N., Crespo, J.L., and Bozhkov, P.V. (2021). Tudor staphylococcal nuclease is a docking platform for stress granule components and is essential for SnRK1 activation in Arabidopsis. EMBO J. *40*, e105043. https://doi.org/10.15252/embj.2020105043.
66. Xie, Z., Zhao, S., Li, Y., Deng, Y., Shi, Y., Chen, X., Li, Y., Li, H., Chen, C., Wang, X., et al. (2023). Phenolic acid-induced phase separation and translation inhibition mediate plant interspecific competition. Nat. Plants *9*, 1481–1499. https://doi.org/10.1038/s41477-023-01499-6.
67. Rezcallah, M.C., Al-Mazi, T., and Ammit, A.J. (2021). Cataloguing the phosphorylation sites of tristetraprolin (TTP): Functional implications for inflammatory diseases. Cell. Signal. *78*, 109868. https://doi.org/10.1016/j.cellsig.2020.109868.
68. Schichl, Y.M., Resch, U., Lemberger, C.E., Stichlberger, D., and de Martin, R. (2011). Novel phosphorylation-dependent ubiquitination of tristetraprolin by mitogen-activated protein kinase/extracellular signal-regulated kinase kinase kinase 1 (MEKK1) and tumor necrosis factor receptor-associated factor 2 (TRAF2). J. Biol. Chem. *286*, 38466–38477. https://doi.org/10.1074/jbc.M111.254888.
69. Huang, L., Yu, Z., Zhang, Z., Ma, W., Song, S., and Huang, G. (2016). Interaction with Pyruvate Kinase M2 Destabilizes Tristetraprolin by Proteasome Degradation and Regulates Cell Proliferation in Breast Cancer. Sci. Rep. *6*, 22449. https://doi.org/10.1038/srep22449.
70. Scinicariello, S., Soderholm, A., Schäfer, M., Shulkina, A., Schwartz, I., Hacker, K., Gogova, R., Kalis, R., Froussios, K., Budroni, V., et al. (2023). HUWE1 controls tristetraprolin proteasomal degradation by regulating its phosphorylation. Elife *12*, e83159. https://doi.org/10.7554/eLife.83159.
71. López-Palacios, T.P., and Andersen, J.L. (2023). Kinase regulation by liquid-liquid phase separation. Trends Cell Biol. *33*, 649–666. https://doi.org/10.1016/j.tcb.2022.11.009.
72. Jang, J.C. (2016). Arginine-rich motif-tandem CCCH zinc finger proteins in plant stress responses and post-transcriptional regulation of gene expression. Plant Sci. *252*, 118–124.
73. Liu, S., and Chen, Z.J. (2011). Expanding role of ubiquitination in NF-kappaB signaling. Cell Res. *21*, 6–21. https://doi.org/10.1038/cr.2010.170.
74. Tenekeci, U., Poppe, M., Beuerlein, K., Buro, C., Müller, H., Weiser, H., Kettner-Buhrow, D., Porada, K., Newel, D., Xu, M., et al. (2016). K63-Ubiquitylation and TRAF6 Pathways Regulate Mammalian P-Body Formation and mRNA Decapping. Mol. Cell *62*, 943–957. https://doi.org/10.1016/j.molcel.2016.05.017.
75. Zavaliev, R., Mohan, R., Chen, T., and Dong, X. (2020). Formation of NPR1 Condensates Promotes Cell Survival during the Plant Immune Response. Cell *182*, 1093–1108.e18. https://doi.org/10.1016/j.cell.2020.07.016.
76. Liu, C., Mentzelopoulou, A., Hatzianestis, I.H., Tzagkarakis, E., Skaltsogiannis, V., Ma, X., Michalopoulou, V.A., Romero-Campero, F.J., Romero-Losada, A.B., Sarris, P.F., et al. (2024). A proxitome-RNA-capture approach reveals that processing bodies repress co-regulated hub genes. Plant Cell *36*, 559–584. https://doi.org/10.1093/plcell/koad288.
77. Updike, D.L., Hachey, S.J., Kreher, J., and Strome, S. (2011). P granules extend the nuclear pore complex environment in the C. elegans germ line. J. Cell Biol. *192*, 939–948. https://doi.org/10.1083/jcb.201010104.
78. Tang, Y., Yang, X., Huang, A., Seong, K., Ye, M., Li, M., Zhao, Q., Krasileva, K., and Gu, Y. (2024). Proxiome assembly of the plant nuclear pore reveals an essential hub for gene expression regulation. Nat. Plants *10*, 1005–1017. https://doi.org/10.1038/s41477-024-01698-9.
79. Ravindran, R., and Michnick, S.W. (2024). Biomolecular condensates as drivers of membrane trafficking and remodelling. Curr. Opin. Cell Biol. *89*, 102393. https://doi.org/10.1016/j.ceb.2024.102393.
80. Liu, D., Riggi, M., Lee, H.O., Currie, S.L., Goodsell, D.S., Iwasa, J.H., and Rog, O. (2023). Depicting a cellular space occupied by condensates. Mol. Biol. Cell *34*, tp2. https://doi.org/10.1091/mbc.E22-11-0519.
81. Bogamuwa, S., and Jang, J.C. (2016). Plant Tandem CCCH Zinc Finger Proteins Interact with ABA, Drought and Stress Response Regulators. PLoS One *11*, e0151574.

STAR★METHODS

KEY RESOURCES TABLE

REAGENT or RESOURCE	SOURCE	IDENTIFIER
Antibodies		
Anti-GFP	Roche	RRID: AB_390913
Anti-RFP	ChromoTek	RRID: AB_2631395
Anti-HA-Peroxidase	Roche	RRID: AB_390917
Anti-FLAG-Peroxidase	Sigma-Aldrich	RRID: AB_439702
Bacterial and virus strains		
Escherichia coli	N/A	DH5α
Escherichia coli	N/A	BL21
Agrobacterium tumefaciens	N/A	GV3101
Chemicals, peptides, and recombinant proteins		
Murashige & Skoog Modified Basal Medium	Phytotech	Cat #M404
Cycloheximide	Sigma-Aldrich	Cat # 01810
MG132	Abcam	Cat # ab141003
PYR41	Sigma-Aldrich	Cat #N2915
GFP-Trap Magnetic Agarose	ChromoTek	RRID: AB_2631358
Critical commercial assays		
SuperSignal West Femto Maximum Sensitivity Substrate	Thermo	Cat # 34095
Experimental models: Organisms/strains		
Arabidopsis thaliana ecotype Colombia	–	–
Arabidopsis: CaMV35S:TZF1-GFP	This paper	N/A
Arabidopsis: CaMV35S:MKK4-GFP	This paper	N/A
Arabidopsis: CaMV35S:MKK5-GFP	This paper	N/A
Oligonucleotides		
Primers used for transient assay and stable lines	Table S2	N/A
Primers used for Y2H	Table S2	N/A
Primers used for BiFC	Table S2	N/A
Recombinant DNA		
Plasmids used in this study	Table S1	N/A

EXPERIMENTAL MODEL AND STUDY PARTICIPANT DETAILS

Plant materials and growth conditions

Arabidopsis thaliana ecotype Columbia (Col-0) was used in this study. The *keg-4* mutant (CS67951) was obtained from the Arabidopsis Biological Resource Center (ABRC). WT, *keg-4*, and transgenic plants were grown in a growth chamber at 22°C with a photoperiod of 16-h light/8-h dark.

METHOD DETAILS

Molecular cloning and generation of transgenic plants

The coding sequence (CDS) of TZF1, MKK4, and MKK5 were cloned into the pENTR/D-TOPO vector. All constructs were subcloned into the Gateway destination binary vector with C-terminal GFP tag by using the LR recombination reaction and then transformed into WT plants by the floral dip method. The constructs used for phosphorylation and ubiquitination mutant analysis were cloned into a modified pBlueKS+ plasmid with LR recombination sites as a Gateway destination vector.[30]

Y2H assay

The CDS of TZF1 was cloned into the pGBKT7 vector and the CDS of MKK4, MKK5, MPK3, and MPK6 were cloned into the pGADT7 vector. Pairs of pGBKT7 and pGADT7 plasmid were co-transformed into the yeast strain AH109 following the Matchmaker GAL4 Two-Hybrid System instructions (Clontech). Primary transformants were selected on synthetic drop-out (SD) medium lacking Trp and Leu and confirmed again by colony PCR before growing on SD medium lacking Ade, His, Trp, and Leu.

Protoplast transient expression and BiFC assays

For transient expression assay in Arabidopsis protoplasts, TZF1, MKK4, MKK5, MPK3, and MPK6 CDS were cloned into the pENTR/D-TOPO vector and then subcloned into the Gateway destination vector with C-terminal GFP tag by using the LR recombination reaction. For BiFC, the CDS of TZF1 was cloned into pA7-YN (containing N-terminal half of YFP) vector and the CDS of MKK4, MKK5, MPK3, and MPK6 were cloned into pA7-YC (containing C-terminal half of YFP) vector.[81] Plasmid pairs were co-transformed into Arabidopsis protoplasts.

Co-IP assay

Total proteins were extracted from Arabidopsis protoplasts co-expressing *TZF1-2xHA* with *GFP-MPK3*, *GFP-MPK6*, *MKK4-GFP*, *MKK5-GFP* or free *GFP*. Extracted proteins were then incubated with equilibrated GFP-trap beads (Chromotek) at 4°C for 2 h under gentle agitation, followed by 3 times of washing with wash buffer (100 mM Tris pH 8.0, 150 mM NaCl, 5 mM EDTA, 10 mM DTT, 0.1% NP-40). Immunoblots were performed using α-GFP (Roche) or α-HA antibodies (Roche).

In vivo ubiquitination assay

Arabidopsis protoplast samples were co-transformed with *2xHA-UBQ* and the GFP-tagged genes of interest and incubated overnight at room temperature followed by a 2 h treatment with 50 μM MG132. After homogenization in 100 μL of IP buffer (100 mM Tris pH 8.0, 150 mM NaCl, 5 mM EDTA, 10 mM DTT, 0.1% NP-40, protease inhibitor cocktail), the GFP-tagged proteins were immunoprecipitated by incubating the extracts with 15 μL of anti-HA magnetic beads (Thermo Scientific) for 2 h at 4°C with gentle shaking. The anti-HA magnetic beads were collected and washed 3 times with wash buffer (100 mM Tris pH 8.0, 150 mM NaCl, 5 mM EDTA, 10 mM DTT, 0.1% NP-40). Immunoblots were performed using α-GFP (Roche) or α-HA antibodies (Roche).

In vitro ubiquitination assay

The *in vitro* ubiquitination reaction was performed in a 30 μL mixture containing 200 ng E1 enzyme (BB-E−304-050, Boston Biochem), 200 ng E2 enzyme (BB-E2-616-100, Boston Biochem), 5 mg His-ubiquitin (BB-U-530, Boston Biochem), 2 mg purified MBP-KEG fusion protein (as E3 enzyme), and GST-TZF1 fusion protein in a reaction buffer that contains 50 mM Tris–HCl [pH 7.6], 2 mM DTT, 5 mM $MgCl_2$, and 2 mM ATP. After 1 h incubation at 30°C in Eppendorf Thermomixer, the reactions were stopped by adding SDS-PAGE sample buffer. Ubiquitinated proteins were detected using ubiquitinh antibody. MBP-KEG was detected by anti-MBP monoclonal antibody and GST-TZF1 was detected by anti-GST monoclonal antibody.

Identification of TZF1 phosphorylation sites by mass spectrometry

To identify TZF1 phosphorylation sites, TZF1-HA was expressed in Arabidopsis protoplasts (concentration of 2×10^5/mL) for 12 h and treated with or without 0.1 μM flg22 for 15 min. Ten mL protoplasts were used to immunoprecipitate TZF1-HA proteins from mock and flg22-treated samples, respectively. Protoplasts were then lysed with lysis buffer (20 mM Tris-HCl, pH 7.5, 100 mM NaCl, 10% glycerol, 0.5 Triton X-100, 1 mM EDTA, 2 mM DTT, 2 mM NaF, and 2 mM Na_3VO_4, and 1× protease inhibitor EDTA-free cocktail) and immunoprecipitated with α-HA magnetic beads (Thermo Fisher). The immunoprecipitated products were separated by 10% SDS-PAGE and stained with GelCode Blue Stain Reagent (Thermo Fisher) for 2 h at 23°C. The TZF1-HA bands were sliced, trypsin-digested, and phospho-peptides were subjected to LC-MS/MS analysis using an Orbitrap QE LC-MS/MS system (Thermo Scientific) at the proteomics core facility of UT Southwestern Medical Center. The MS/MS spectra were analyzed with Mascot software, and the identified phosphor-peptides were manually inspected to ensure the accuracy of phosphorylation sites detection.

Accession numbers

The accession numbers used are as follows: TZF1 (At2g25900), DCP1(At1g08370), DCP2 (At5g13570), DCP5 (At1g26110), Caprin (At1g27090), G3BP (At5g43960), UBP1b (At1g17370), KEG (At5g13530), MKK4 (At1g51660), MKK5 (At3g21220), MPK3 (At3g45640), and MPK6 (At2g43790).

QUANTIFICATION AND STATISTICAL ANALYSIS

Data are presented as means ± *SE*. Analysis of significances was done using Student's t test. Significance levels (*p* values) are indicated in legends of each figure, showing *, $p < 0.05$.